A&A 506, 1319–1333 (2009)
DOI: 10.1051/0004-6361/200810526

Astronomy & Astrophysics

Properties and nature of Be stars⋆,⋆⋆

26. Long-term and orbital changes of ζ Tauri

D. Ruždjak[1], H. Božić[1], P. Harmanec[2], R. Fiřt[3], P. Chadima[2], K. Bjorkman[4], D. R. Gies[5], A. B. Kaye[6], P. Koubský[7], D. McDavid[8], N. Richardson[5], D. Sudar[1], M. Šlechta[7], M. Wolf[2], and S. Yang[9]

[1] Hvar Observatory, Faculty of Geodesy, University of Zagreb, 10000 Zagreb, Croatia
e-mail: rdomagoj@geof.hr
[2] Astronomical Institute of the Charles University, Faculty of Mathematics and Physics, V Holešovičkách 2, 180 00 Praha 8, Czech Republic
[3] Mathematical Institute, University of Bayreuth, 95447 Bayreuth, Germany
[4] Ritter Observatory, MS 113, Department of Physics and Astronomy, University of Toledo, OH 43606, USA
[5] Center for High Angular Resolution Astronomy, Department of Physics and Astronomy, Georgia State University, PO Box 4106, Atlanta, GA 30302-4106, USA
[6] Department of Physics and Astronomy, George Mason University, Fairfax, Virginia 22030, USA
[7] Astronomical Institute of the Academy of Sciences, 251 65 Ondřejov, Czech Republic
[8] Department of Astronomy, University of Virginia, PO Box 400325, Charlottesville, VA 22904-4325, USA
[9] Physics & Astronomy Department, University of Victoria, PO Box 3055 STN CSC, Victoria, BC, V8W 3P6, Canada

Received 4 July 2008 / Accepted 24 August 2009

ABSTRACT

Context. One way to understand the still mysterious Be phenomenon is to study the time variations of particular Be stars with a long observational history. ζ Tau is one obvious candidate.
Aims. Using our rich series of spectral and photometric observations and a critical compilation of available radial velocities, spectrophotometry of Hα, and *UBV* photometry, we characterize the pattern of time variations of ζ Tau over about a century. Our goal is to find the true timescales of its variability and confront them with the existing models related to various aspects of the Be phenomenon.
Methods. Spectral reductions were carried out using the IRAF and SPEFO programs. The HEC22 program was used for both photometric reductions and transformations to *UBV*. Orbital solutions were derived with the latest publicly available version of the program FOTEL, period analyses employed both the PDM and Fourier techniques – programs HEC27 and PERIOD04.
Results. We derived a new orbital ephemeris $T_{\mathrm{RVmax.}}$ = HJD (2447025.6±1.8) + ($132^{\mathrm{d}}.987$ ±$0^{\mathrm{d}}.050$) ×*E*. The analysis of long-term spectral and light variations shows a clear correlation between the RV and *V*/*R* changes, and a very complex behaviour of the light changes. The character of the orbital light and *V*/*R* changes varies from season to season.

Key words. stars: early-type – binaries: spectroscopic – stars: emission-line, Be – stars: individual: ζ Tauri

1. Introduction

In spite of strong efforts by several generations of observers and theoreticians, the very nature of the Be phenomenon and the causes of (mostly unpredictable) spectral and light variability of individual Be stars remain unexplained. This is obviously caused by the fact that Be stars vary on at least three distinct time scales – see, e.g. Harmanec (1983) – and these variations mutually interfere in a complex manner. Without really long and systematic series of spectral and photometric observations it is almost impossible to distinguish the variations on different time scales properly. This is why we believe that detailed studies of individual Be stars which have rich observational histories represent one important way to address this long-standing problem.

In this paper, we apply such an approach to the bright Be star ζ Tau. The purpose of our study is manifold:

1. To assemble all available spectroscopic, spectrophotometric, photometric, and interferometric observations on ζ Tau and to homogenize them as much as possible. This is described in Sects. 2 and 3 and detailed in Appendixes A and B of this paper. Those data will be published in a follow-up paper containing the alternative model of long-term *V*/*R* changes.
2. To present the first truly comprehensive examination of the long-term variations in a Be star, identify the individual patterns, and examine the relationships between the spectroscopic and broad-band photometric changes (cf. Sect. 4).
3. To study the variations related to the binary nature of ζ Tau. To this end, we used (in Sect. 5) several different techniques of data prewhitening for the long-term changes to provide a convincing proof that the Be star with its envelope moves in a binary orbit with an unseen secondary. We also derived an improved ephemeris and the binary orbital elements and demonstrated a complex character of the phase-locked light

⋆ Based on new spectral and photometric observations from the following observatories: Dominion Astrophysical Observatory, Fairborn, Haute Provence, Hvar, Limber, McDonald, Ondřejov, and Ritter.
⋆⋆ Appendices are only available in electronic form at http://www.aanda.org

and V/R changes. By V/R we mean the ratio of the intensities of violet $I_V \equiv V$ and red $I_R \equiv R$ emission peaks of double peaked emission lines measured in the units of continuum level.

In follow-up paper we plan to present an alternative scenario, namely a blob of material put into orbit around the B star, based on 3-D non-linear hydrodynamical modelling. Since the existing modelling of the long-term V/R changes dealt mainly with the model of the gradually elongated envelope, identified in physical terms with one-armed oscillations in the disk (Johnson 1958; McLaughlin 1961; Okazaki 1997; Fiřt & Harmanec 2006), we plan to present an alternative scenario of a discontinuous blob of material put into the orbit around the B star when applied to "real star" having a quadrupole term in its gravitational potential.

Although quite extensive, our dataset *is not suitable* to a detailed study of *rapid* spectral and light changes since it contains only a very few whole-night series of observations or simultaneous observations from observatories with a large difference in local time. For that reason we plan to obtain new dedicated observations and postpone a detailed study of rapid changes for later.

The final conclusions of this paper are summarized in Sect. 7.

2. Relevant observational facts about ζ Tau

The star ζ Tau (HD 37202, 123 Tau, HR 1910, HIP 26451) is one of the brightest Be stars in the northern sky ($V = 2^{\rm m}.7$–$3^{\rm m}.2$ var.), exhibiting spectral, brightness and colour variations on several distinct time scales. It is also a spectroscopic binary with an orbital period of $132^{\rm d}.97$ days. Its orbital radial-velocity (RV hereafter) variations are superimposed on the cyclic long-term ones. ζ Tau also exhibits the long-term V/R and emission-line strength changes.

2.1. RV variations

The RV variations of ζ Tau were first discovered by Frost & Adams (1903), and Adams (1905) demonstrated that these variations are periodic and concluded that ζ Tau is a spectroscopic binary with an orbital period of 138 days. Losh (1932) improved the value of the period to 133 days, but reported also long-term RV variations in addition to the periodic ones. Since that time a large number of spectroscopic studies of ζ Tau were carried out, for instance by Hynek & Struve (1942), Underhill (1951, 1952), Miczaika (1953), Aydin et al. (1965), Delplace (1970a,b), Abt & Levy (1978), Harmanec (1984), Jarad (1987), Mon et al. (1992), Guo et al. (1995), Rivinius et al. (2006), Pollmann & Rivinius (2008), and Štefl et al. (2009), among others. Thanks to these studies it became clear that in certain time intervals simple orbital RV changes are observed (with a full amplitude of some 15 km s^{-1}) while in others cyclic long-term changes with variable cycle lengths (roughly between 4 and 7 years) and a full amplitude up to 150 km s^{-1} are superimposed on the orbital RV changes.

Harmanec (1984) compiled all RVs available at that time, removed long-term changes via spline functions, and derived the most accurate orbital ephemeris

$$T_{\rm upper\,conj.} = {\rm HJD}\ 2415549.638 + 132^{\rm d}.9735 \times E\,, \qquad (1)$$

which has then been adopted in the majority of consecutive studies. Harmanec (1984) and Floquet et al. (1989) concluded that ζ Tau consists of a 11 $M_\odot$ primary and a 1.3 $M_\odot$ secondary. In all probability, the secondary *is not filling* its Roche lobe, and it might be a hot compact object similar to that found for φ Per (Gies et al. 1998). However, no direct observational evidence of a hot companion is available.

2.2. Spectral variations

Losh (1932) and Lockyer (1936) reported the presence of cyclic V/R variations on a time scale of several years as well as long-term line-strength changes.

Delplace (1970b) was probably the first one to point out that the Balmer emission-line profiles are not always the usual double-peaked emissions but can be more complicated – see her Fig. 6. Depending on how one wants to interpret them, the profiles adopt a shape of either three or even four distinct emission peaks or emission with two or even three separate absorption cores. Delplace (1970b) pointed out that these complicated profiles appear only at specific phases of the long-term RV and V/R cycle. Rivinius et al. (2006), Štefl et al. (2007), Pollmann & Rivinius (2008), and Štefl et al. (2009) confirmed the presence of such complicated Hα line profiles in their electronic spectra. They argued that such profiles are observed when the V/R is close to one, but only on the rising branch of the V/R curve.

2.3. Light and colour changes

Contrary to numerous spectroscopic observations, there are no systematic photometric observations of ζ Tau published before 1980. The first report about possible variability was by Köllnig-Schattschneider (1940) who observed ζ Tau during six nights in 1940. Haupt & Schroll (1974) found a decrease in light of some $0^{\rm m}.2$ during 1968–1969. Hubert-Delplace et al. (1982) were the first to note that a broad light minimum recorded in the 13-colour system in the second half of the seventies (Alvarez & Schuster 1981; Schuster & Alvarez 1983) coincides with the long-term V/R maximum and also a RV maximum which was documented in detail by Hubert-Delplace et al. (1983). The same correlation was also noted for another long-term cycle by Vakili et al. (1998). First measurements in the *UBV* system were secured at Hvar Observatory in the winter of 1976/1977 and revealed a steady $0^{\rm m}.1$ decrease in V during the observations.

A systematic monitoring of ζ Tau at the Hvar Observatory started in 1981 and the first results were published by Pavlovski & Božić (1982). Božić & Pavlovski (1988) classified the light variability of ζ Tau into three types:

(1) long-term variations on the scale of years;
(2) occasional orbital phase-locked light changes that were present in some cycles;
(3) 0.8 day (or 1.6 day) rapid light variations with period and amplitude slightly varying in time.

A more extensive set of observations was reported in Pavlovski et al. (1997). Photometric variations were also studied by Bossi & Guerrero (1989), Percy et al. (1994) who advocated periods of rapid changes in the range between $0^{\rm d}.65$ and $0^{\rm d}.85$, and by Guo et al. (1995).

The behaviour of the colour indices of ζ Tau in time and in the colour-colour diagram was briefly described by Pavlovski et al. (1997). Both indices show variations of $\sim 0^{\rm m}.1$. In the $(U-B)$ vs. $(B-V)$ diagram, the colour variations of ζ Tau correspond to an apparent transition from the main sequence to the giant branch and back.

2.4. Interferometric observations

More recently, the star was observed with several optical interferometers which are capable of resolving the envelope around it (Quirrenbach et al. 1994, 1997; Vakili et al. 1998). Using the Navy Prototype Optical Interferometer, Tycner et al. (2004) found that emission-line envelope which surrounds the primary star is well inside the Roche lobe around it. Gies et al. (2007) analyzed the most recent near-IR interferometric observations in the K band and concluded that the emission disk is viewed almost edge-on.

3. Observational material used

We compiled a large collection of radial velocities, spectrophotometric quantities and photometric observations for which dates of observations were available from the astronomical literature. Most of the RVs were previously compiled by Harmanec (1984), but we have critically revised these data and checked them with their original sources. In addition, we obtained and reduced a very large number of spectral and photometric observations ourselves. A detailed discussion of all observational data, their reduction and journals of observations are provided in Appendix A (spectroscopy) and B (photometry).

Here we only mention some important points relevant to further analyses.

Electronic spectra at our disposal mainly cover the red part of the spectrum containing the Si II 6347 and 6371 A doublet, Hα and He I 6678 A. To be able to study both the orbital motion and the long-term changes in the envelope, we measured RVs of the steep emission wings of Hα, of the broad He I 6678 A wings and also of the shell absorption cores of Hα, He I 6678 A, and the Si II 6347 and 6371 A lines.

Since ζ Tau frequently displays a rather complicated Hα profile (Delplace 1970b; Rivinius et al. 2006), special attention was paid to the determination of the V/R ratio of its emission peaks. Besides "ordinary", double-peaked emission lines, in about 30% of high-resolution spectra triple-peaked Hα profiles are seen and on several occasions both emission peaks are divided in two so the quadruple-peaked profiles are observed. This is probably due to the presence of additional absorption components in the Hα line, caused by complicated and possibly non-Keplerian kinematic structure in the disc. In approximately 25% of the profiles the second absorption component is seen, but no distinct third peak was formed and the resulting double-peaked profile has one distinctly asymmetric peak (see for instance the lowest profile in Fig. 1). Sometimes, one sees a more or less central emission peak and two fainter ones located on both sides from it. In Fig. 1 a sequence of complicated profiles is shown. A gradual transition from asymmetric, double-peaked profiles to the triple-peaked ones and vice versa can be seen there. Such complicated profiles make the determination of the V/R ratio difficult or even meaningless.

To handle this problem, we split the dataset into two subsets, according to the observed Hα profile. One subset consists of *simple profiles* by which we mean double-peaked profiles and/or profiles with only one absorption core. The second subset contains *complex profiles*, i.e., asymmetric double-peaked and multi-peaked profiles or profiles with more than one absorption core.

We measured peak and core intensities of all parts of the complicated profiles. To obtain an estimate of the V and R peak intensities and of the V/R ratio, we derived the position of the centre of the whole emission profile at an arbitrarily chosen intensity of 1.5 (in the units of continuum level). We then averaged the measured intensities of all peaks to the left of this centre to obtain the value of V and to the right of it to obtain R and calculated the V/R ratio from these estimates. Note that while some authors use the notation V and R to denote the intensities of the emission peaks *only above* the continuum level, our values are consistently measured from zero intensity level[1]. We converted the data compiled from the literature – if necessary – into our type of measurement. Additionally, for complex profiles we measured RVs of three separate absorption components: red, violet and central.

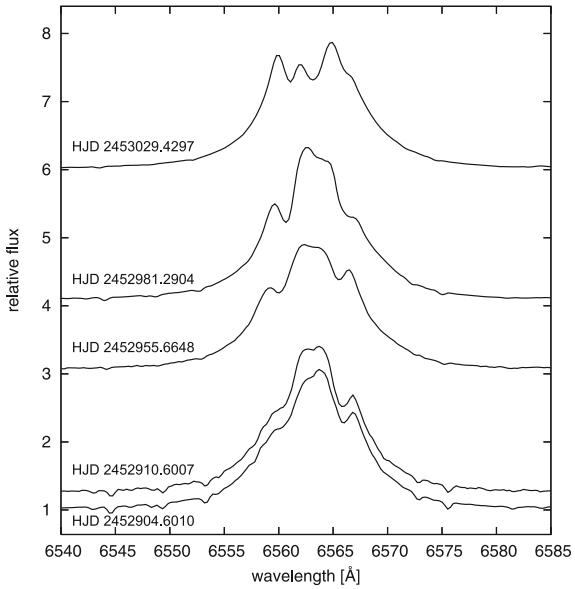

Fig. 1. Sequence of Hα profiles observed in Ondřejov between 2003, Sept., 22 02:24 UT and 2004, Jan., 24 21:57 UT (125 days). The HJDs of individual profiles are given and the vertical offset of the profiles is proportional to time in such a way that one unit of relative continuum flux corresponds to 25 days. (Note the feature moving across the top of the profile).

4. Long-term changes

A plot of various observables vs. time, based on *individual* data points, is shown in Figs. 2a–2f. It is obvious that all measured spectral and photometric quantities exhibit pronounced long-term variations but also variations on shorter time scales. The interpretation of long-term changes is by no means straightforward. The problem is that the long-term variations are affected by at least two independent processes: by long-term changes of the extent and density of the envelope (usually detected via the so-called E/C changes, i.e., changes in the ratio of intensity of the emission lines to the neighbouring continuum) and by the precession of an elongated non-axisymmetric envelope (which manifests itself by the V/R changes).

From Fig. 3, we see that over the last 100 years, ζ Tau has gone through three "active" stages characterized by pronounced long-term RV and V/R variations and two "quiet" stages in which the RV and V/R variations are less pronounced. During the active stages, the Hα emission tended to be very strong, (i.e., it had a larger equivalent width); during quiet stages, Hα emission profiles were less pronounced (cf., e.g., Figs. 2b and 2c).

[1] Thus, for instance, where our measured peak value is, say, F_p/F_c = 1.7 (where F_p and F_c are the peak and continuum fluxes, respectively), then in the alternative notation the peak value is $(F_p–F_c)/F_c$ = 0.7.

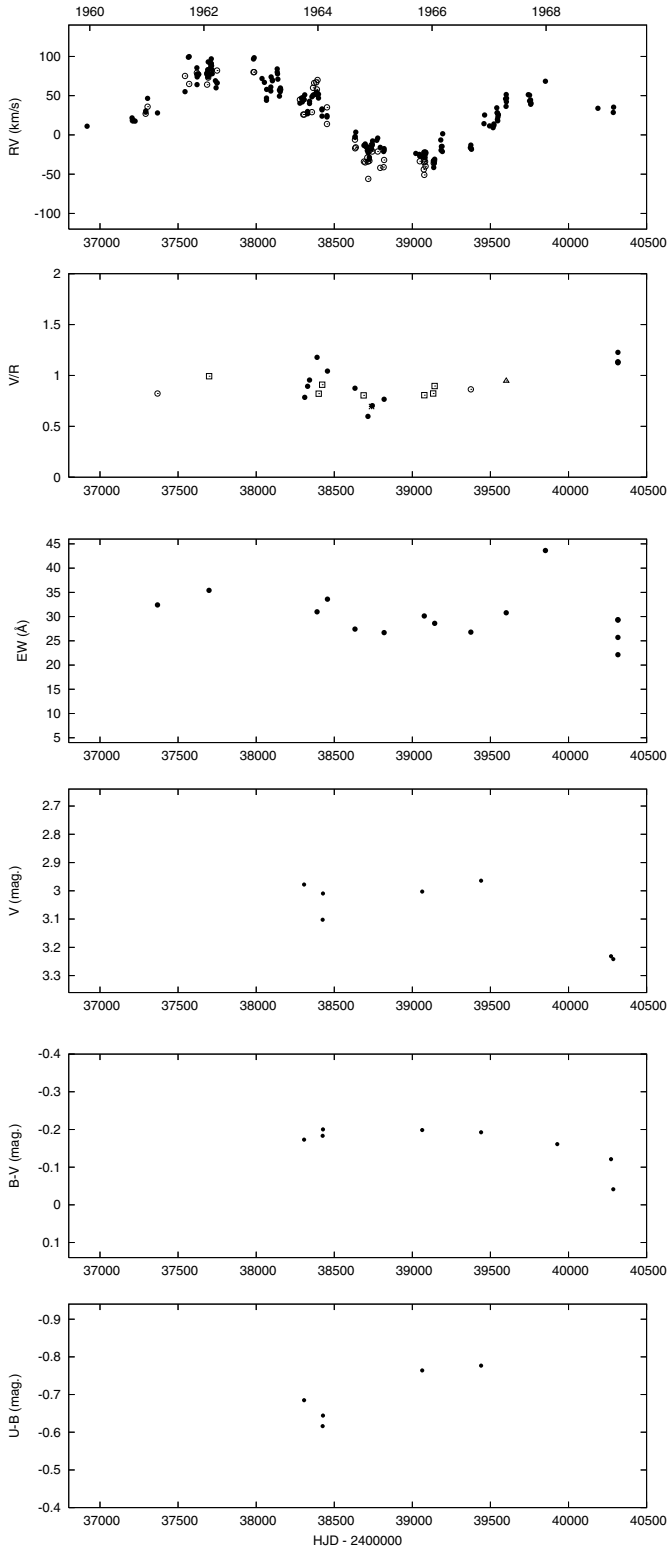

Fig. 2a. Long-term RV, V/R, Hα emission strength, brightness and colour variations of ζ Tau during time interval HJD 2436800–2440500. Different symbols on RV plots denote: H I shell – filled circles, He I shell – empty circles and Si II shell – squares. In the V/R plots, filled circles denote simple double-peaked profiles, empty circles the triple-peaked ones, squares the asymmetric double-peaked ones, triangles the quadruple-peaked ones, and asterisks the unclassified profiles. Note that strong emission is defined by positive equivalent width in this instance. A typical rms error of a single Hvar (most numerous data set) photometric observation is $0^{m}.01$.

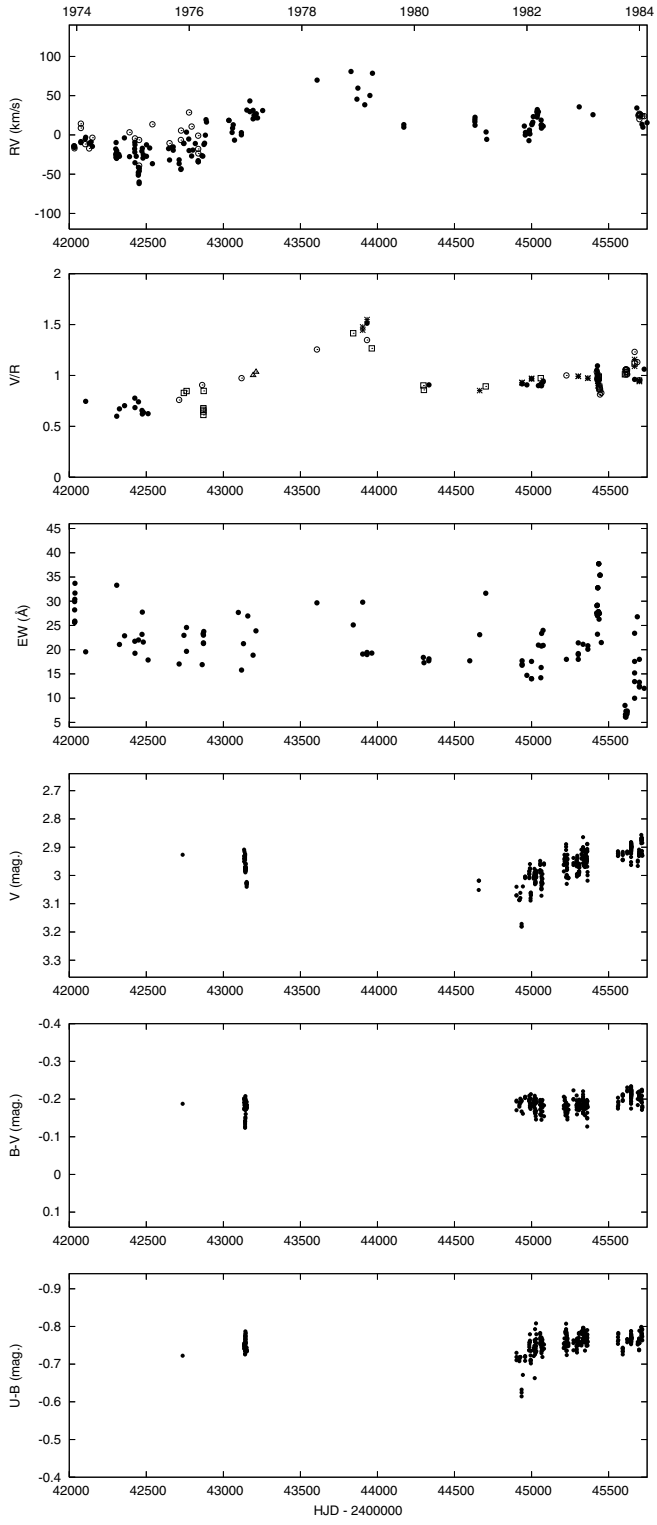

Fig. 2b. The same as Fig. 2a for the time interval HJD 2442000–2445750.

Although the time coverage by different types of observations is less complete than what one would like to have, it seems from an inspection of Figs. 2a–2f that some patterns are emerging:

1. During all intervals when the long-term RV and V/R changes were present, they always vary in phase (Hubert-Delplace et al. 1983; Hubert et al. 1987; Mon et al. 1992).

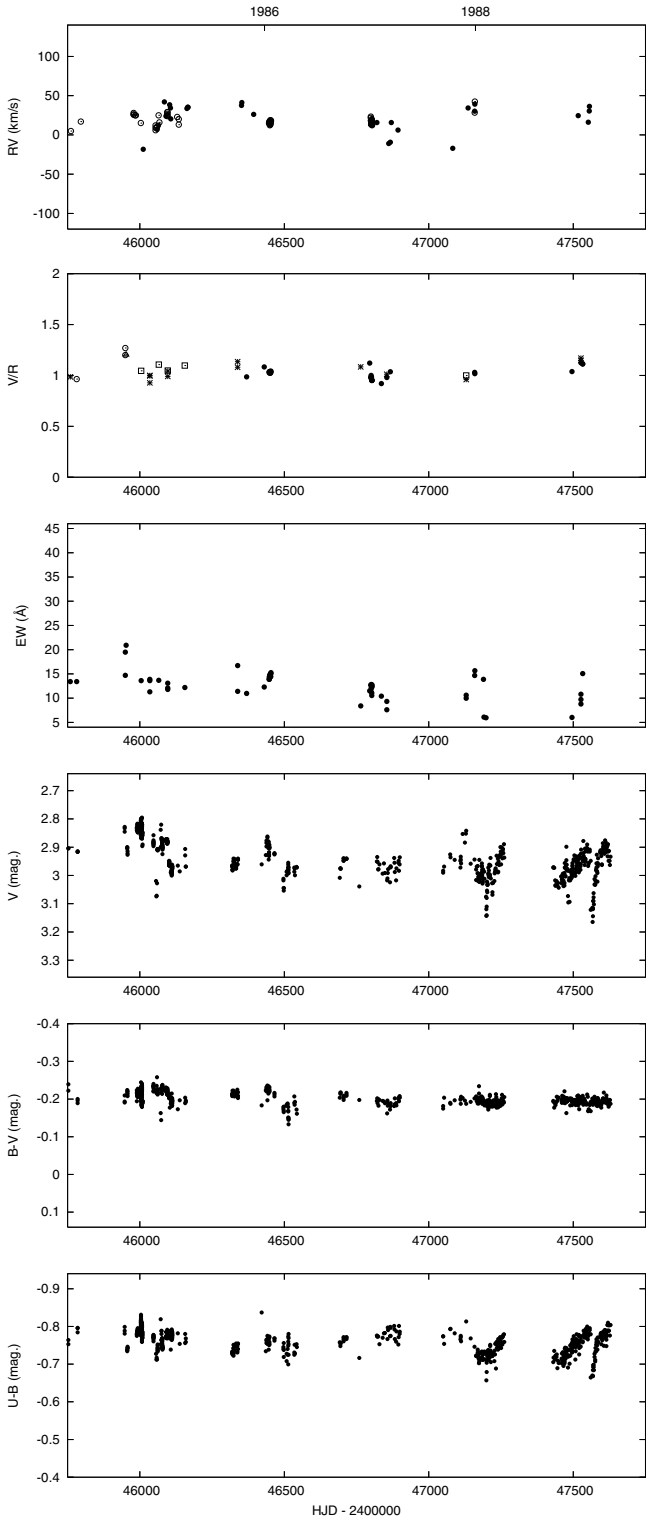

Fig. 2c. The same as Fig. 2a for the time interval HJD 2445750–2447750.

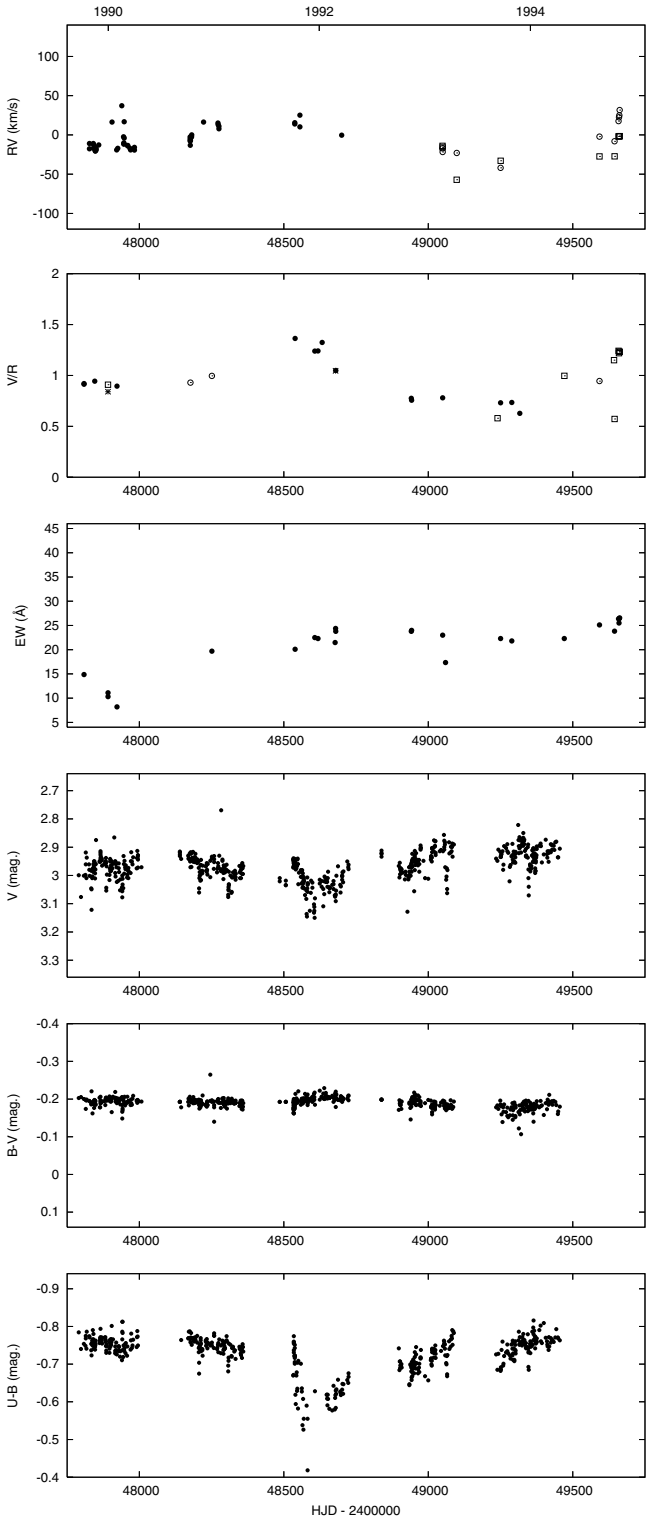

Fig. 2d. The same as Fig. 2a for the time interval HJD 2447750–2449750.

2. Already Hubert-Delplace et al. (1982) and Vakili et al. (1998) noted that the minimum brightness occurred near RV and V/R maxima on two different occasions. It seems, however, that the behaviour is more complex in fact. We note that during the time interval JD 2436800–JD 2440500 also the EW varies in phase with the RV changes. However, in the recent long-term cycles (JD > 2 448 000), changes of the Hα EW are not in phase with the RV changes. Mennickent et al. (1997) classified ζ Tau as a star for which occultations of the stellar disk by the density enhancement due to one-armed oscillation should be observable on the descending branch of the long-term V/R cycles. As Figs. 2a–2f show, the needed parallel V/R and photometric data are missing. The only case where such a light decrease could be suspected is

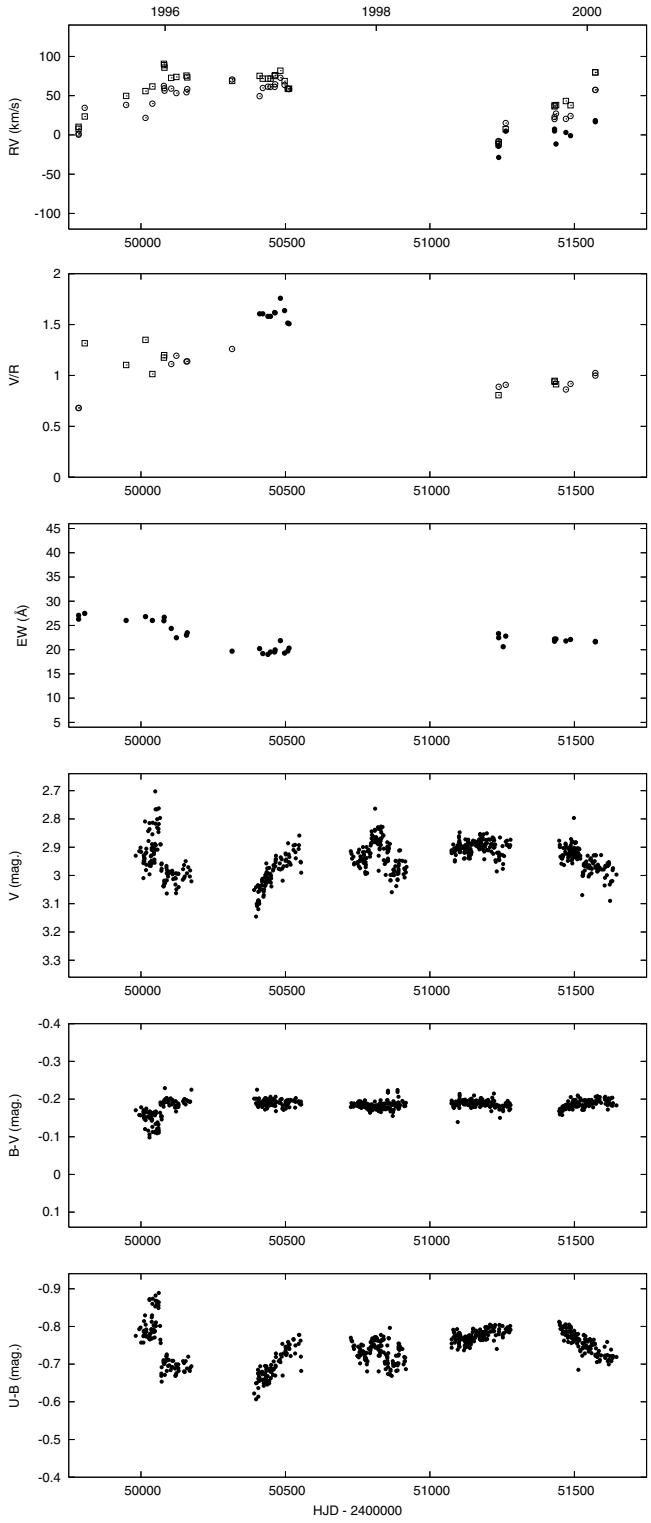

Fig. 2e. The same as Fig. 2a for the time interval HJD 2449750–2451750.

the time interval around JD 2453600 but photometry is very scarce there.

3. The light variations are obviously quite complex and one can note a rather frequent occurrence of sharp light decreases lasting typically some 10–20 days. Notably, they are quite pronounced over the time interval between HJD 2446000–2448000 when the long-term activity more

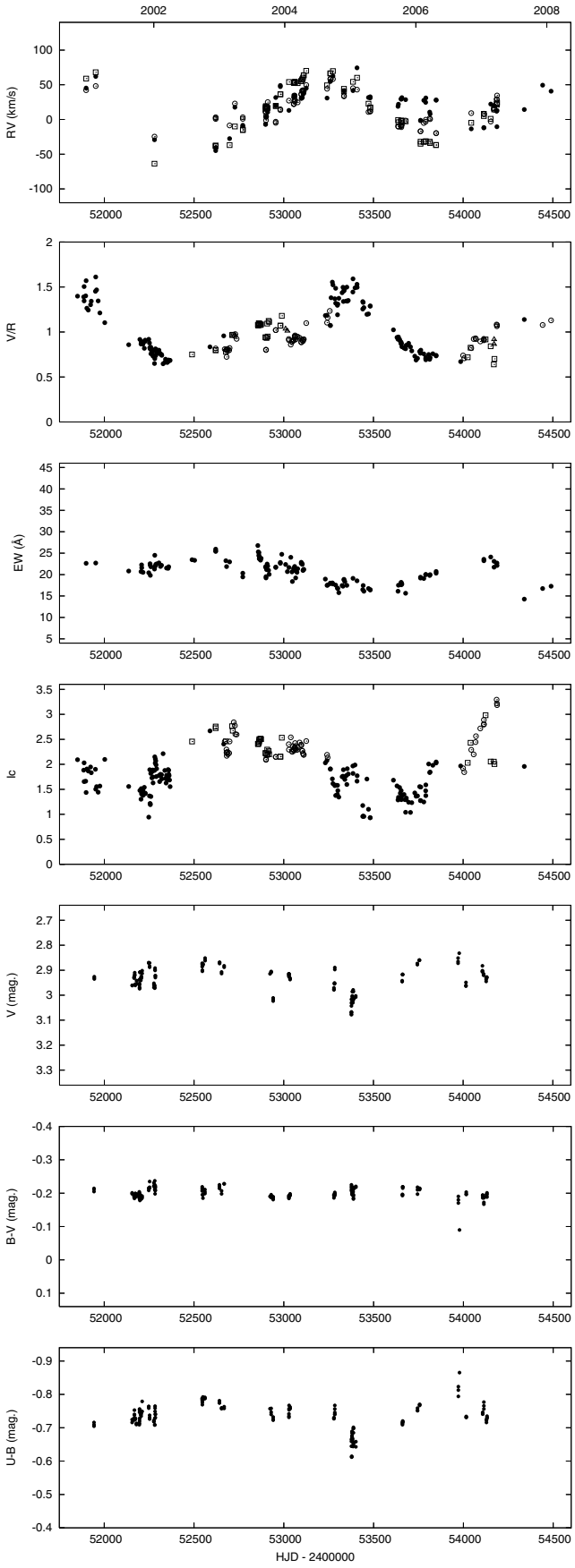

Fig. 2f. The same as Fig. 2a for the time interval HJD 2451750–2454600. Additionally, the central intensity of the Hα absorption core is shown. The same symbols are used in this plot as for the V/R ratio.

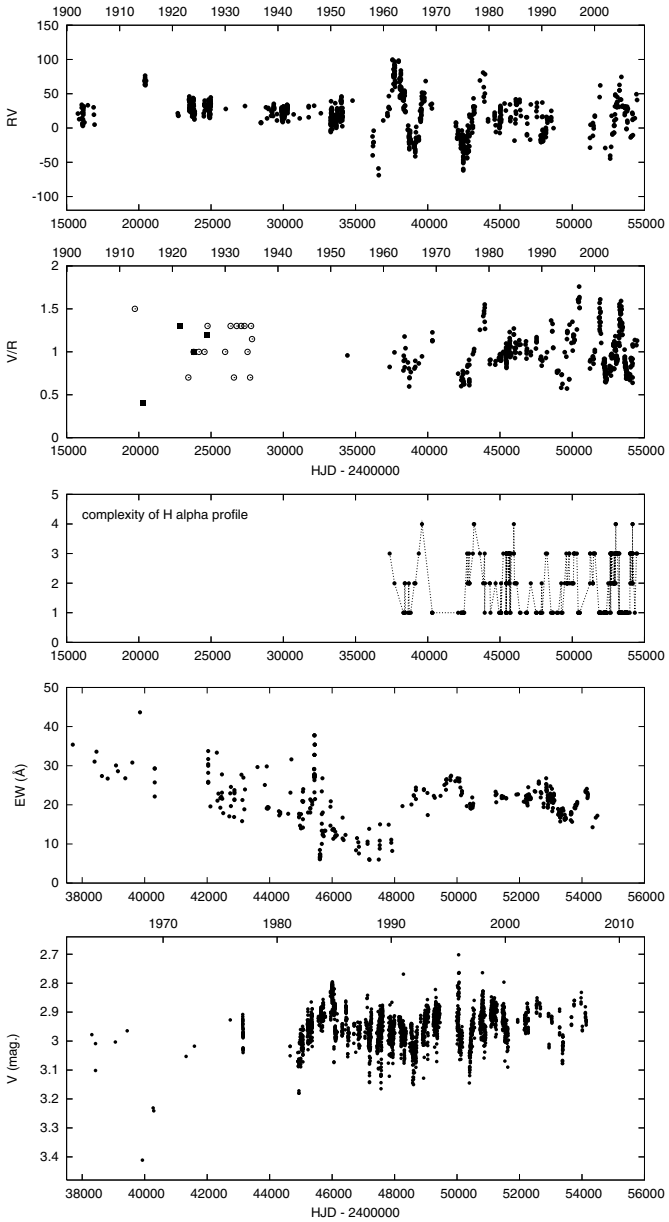

Fig. 3. Long-term variation of the H I shell RVs, the V/R ratio of the Balmer emission lines of ζ Tau, and the complexity of the emission profiles (measured by the number of apparent emission peaks of Hα) over a time interval of about 100 years shown together with long-term Hα equivalent width and brightness variations over a time interval of about 50 years. (Note the different time scale of this plots which was used to improve the visibility of the changes.) In the V/R plot filled circles denote measurements for Hα, filled squares those for Hβ taken from Losh (1932), and empty circles the estimates by Lockyer (1936).

or less disappeared – see also Mon et al. (1992), Ballereau et al. (1992), and Guo & Guo (1992) for the description of this interval without long-term changes. The light decreases occur in different orbital phases of the binary, not only during the binary conjunctions as originally conjectured by Božić & Pavlovski (1988). These light decreases are not accompanied by any notable changes of the $B-V$ colour but are seen as a reddening in $U-B$. The only notable change of $B-V$ colour is reddening up to $0^{m}.1$ around HJD 2450000 which takes place when the RV of the shell lines exceeds approximately

Table 1. Slopes obtained by linear regression ($y = a\,x + b$) for V magnitude and Hα EW data for all available data and several subsets.

HJD–2400000	N	$a_{V\,\mathrm{mag.}}$	N	a_{EW}
all data	2465	–0.85 ± 0.53	382	–0.169 ± 0.075
HJD < 49000	1529	9.0 ± 1.2	206	–1.89 ± 0.20
47750 < HJD < 48750	375	60.4 ± 7.7	11	14.5 ± 2.0
HJD > 49000	936	0.8 ± 1.5	176	–0.94 ± 0.14

The coefficients are expressed in units of micromagnitude per day and miliangström per day.

50 km s^{-1} for the first time since the beginning of new active phase.

4. The pattern of the long-term light changes is less clear due to the fact that the light changes on shorter time scales are quite pronounced. The general impression from the plot of V magnitude shown in Fig. 3 is that the brightness of ζ Tau at the recorded brightness maxima has been slowly increasing over the whole time interval of 44 years covered by available photometry with known times of observations. Such an impression is corroborated by the results of linear regression presented in Table 1. The result for all available data, although not statistically significant, shows that the brightness has been increasing during last 44 years. The results for several selected subsets are somewhat confusing and indicate that both, the mild secular decreases, as well as the large increase of EW in the period JD 2447750–2448750 are accompanied by the decrease of the brightness.
5. The beginning of a new active phase more or less coincides with the extensive use of electronic spectra and some correlations can be studied in more detail – see Fig. 2f. As clearly seen in Fig. 3, the complicated Hα profiles with several absorption cores are *always only observed on the rising branch of the V/R cycle*, as first noted by Delplace (1970b) and Rivinius et al. (2006). The increased accuracy of more recent data (shown in Fig. 2f) allows us to conclude that the emission strength also exhibited some cyclic changes during the last V/R cycle, attaining maximum when complex profiles are observed, i.e., in the middle of the rising branch of the V/R cycle. Also, note that the depth of the Hα shell core is lowest at the same time, i.e., the line intensity measured from the zero level in the rectified spectra is maximum – see panel I_c in Fig. 2f. It can be concluded that the complex profiles are observed when the shell lines become weak and multiple, which contributes to the increase of the equivalent width of the emission profile.

The appearance of complex profiles can be explained by presence of additional emission or absorption components. The increased value of Hα EW suggests the presence of additional emission components, which then rises the question: From where does this extra emission originate. However, there are several arguments that the complex profiles are caused by additional absorption components. First, measured RVs of all additional absorption components in Hα exhibit identical long-term variations as the shell lines and they move with the star, indicating that in the most cases they are genuine absorptions, not just gaps between two neighbouring emission peaks. Next, the mean value of Hα EW for all complex profiles in our sample does not differ significantly from the mean value for all simple profiles (21.63 ± 0.49 vs. 20.23 ± 0.41 respectively) in contrast to what would be expected if extra emission exists. Finally, the complex profiles are observed when the density enhancement is passing behind the star and if the inclination is high one can speculate

that these absorptions arise in some circumstellar material which is occulted by the density enhancement on the descending part of the V/R cycle. For instance if the density perturbation has the spiral shape and it is not confined to the inner part of the disc, the passage of the inner part of the perturbation behind the star would coincide with the passage of outer part of perturbation in front of the star and vice versa.

The behaviour of ζ Tau in the $(U-B)$ vs. $(B-V)$ diagram is shown in Fig. 4. In the top panel, the data from the time interval HJD 2438306–2447630 are shown, but the systematic observations started roughly round HJD 2445000. During this period (HJD 2445000–2447630) there are no long term RV and V/R variations, i.e., the circumstellar disc is symmetrical and it is slowly dispersing. Looking at Figs. 2b and 2c, it is evident that the changes in $B-V$ occur on short time scales. Those obviously reflect short-term changes in the inner disk. Also, if the star is partially screened by the disc, the decreasing radius and/or density of the disc will result in the increase of brightness and a tendency for $B-V$ and $U-B$ to become more blue due to a decrease of absorption and scattering of the light in the disc. On the other hand, the depletion of the disc will result in a decrease of emission from the disc itself what will result in a brightness decrease, bluer $B-V$ and redder $U-B$. Therefore depletion of the disc results in $B-V$ changes while $U-B$ and brightness remain roughly constant, and this is manifested in the colour-colour diagram as horizontal movement.

Around HJD 2448000 the Hα EW reaches a minimum and starts to increase. This increase coincides with the onset of the long-term RV and V/R variations, i.e., the increasing density and/or diameter of the disc coincides with development of an asymmetry in the disc. The increase of emission is accompanied with a decrease of brightness and redder $U-B$ colour index (cf. Table 1 and Fig. 2d). This type of behaviour is typical for the inverse correlation between the H I emission strength and the luminosity as defined by Harmanec (1983). However, no reddening of $B-V$ is seen. The effect is more pronounced due to the minimum of brightness and $U-B$ colour index which occurs immediately after the first maximum of the long-term cycle (round HJD 2448500). This may be caused by the transit of a newly formed density enhancement in front of the star, i.e., when the densest part of asymmetrical disc is projected to stellar surface. This minimum is denoted by empty symbols in the second panel of Fig. 4.

As already pointed out, the only notable change of the $B-V$ colour is a reddening up to $0^{\rm m}.1$ that occurred between HJD 2450000 and 2450100. The change consists of few sharp reddenings which are accompanied by blueings of the $U-B$ colour and increases of brightness. This is a signature of the positive correlation as defined by Harmanec (1983). It is illustrated in the third panel of Fig. 4. Those changes take place when RV of the shell lines exceed some 50 km s^{-1} prior to maximum of long-term cycle, i.e., when newly formed density enhancement becomes visible after passing behind the star.

In the remaining panel, the data from time interval HJD 2448897–2454131 are shown (with the data HJD 2450000–2450100 excluded there). It can be seen that the colour behaviour in this time interval is complex and reminiscent of a positive correlation.

It can be concluded that overall behaviour of ζ Tau in the colour-colour diagram does not consistently show either a positive or an inverse correlation between the H I emission strength and the luminosity. This kind of behaviour is typical for stars with intermediate inclination, where the inhomogeneous structure of the disc and changing rate of screening will disturb the simple correlation between the H I emission strength and the luminosity; see, e.g., κ Dra (Juza et al. 1994) and 4 Her (Koubský et al. 1997). On the other hand, the estimated inclination of ζ Tau is in the range of 67° to 87°, too high to support this picture.

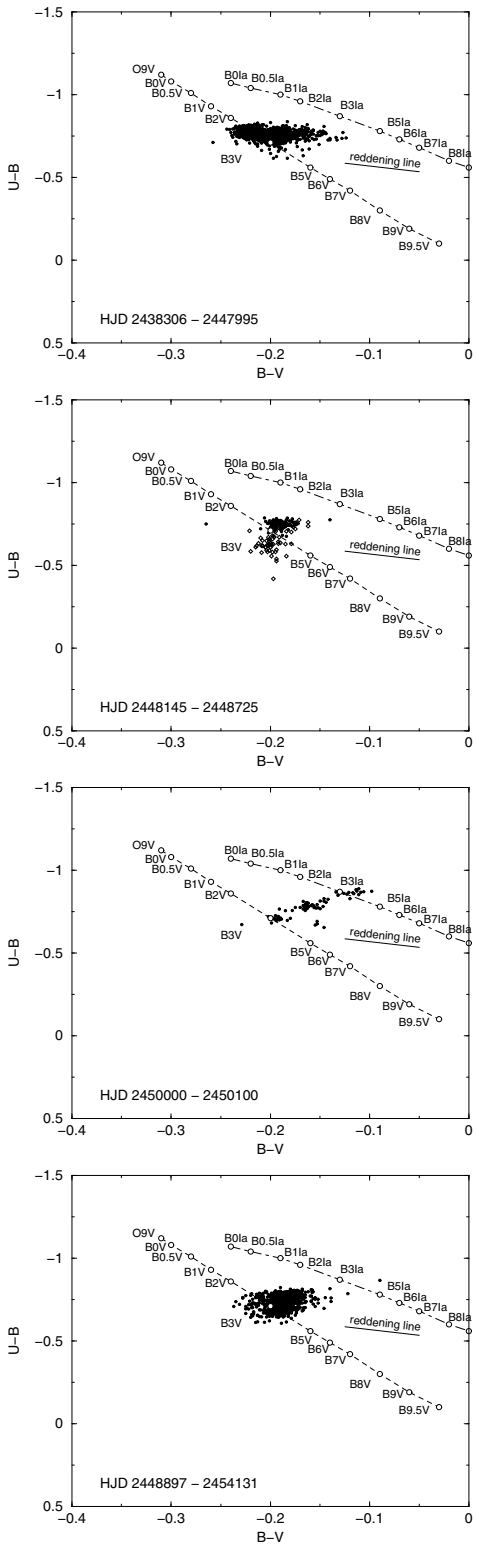

Fig. 4. The $(U-B)$–$(B-V)$ colour diagram with the main and supergiant sequences shown. Individual *UBV* observations are plotted. The time intervals are denoted on the plots and the data from HJD 2450000–2450100 are excluded from the bottom plot.

5. Orbital changes

5.1. RV changes, orbital solutions and a new ephemeris

The determination of reliable orbital RV curves of Be stars which are members of binary systems is difficult due to presence of variations on several different timescales. This is reflected in the determination of their correct orbital elements.

The RV curves based on the sharp shell absorption lines are often affected by asymmetries which result in RV curves with sharp maxima and flat minima, reminiscent of eccentric orbits with the longitude of periastron near 0° – see, e.g., Fig. 3 in Harmanec (1985), for numerous examples of such curves. The RV curves of the rotationally broadened He I lines, supposed to originate in the stellar photosphere – or at least in the densest inner parts of the envelope close to the true photosphere – usually show a very large scatter around the mean RV curve. This additional scatter is probably caused by the rapid line-profile variations. Harmanec et al. (2002b) argued that the RV curves of Be star binaries, based on He I line profiles, might be affected by the phase-locked V/R changes, and that this may lead to the overestimation of the orbital semi-amplitudes. That this is indeed the case for several studied Be binaries (γ Cas, φ Per, κ Dra, V839 Her and V832 Cyg) was shown in Harmanec (2003).

Following Božić et al. (1995), we measured the steep wings of the strong Hα emission to obtain the most realistic estimate of the orbital motion of the B primary. This approach led to the determination of orbital RV curves for several other Be binaries (see Harmanec (2003) and references therein). The reasons why it should be so are the following:

1. any available models of the disks indicate that their outer parts rotate more slowly than their inner parts;
2. it is very probable that at least the denser inner parts of the disk in a binary system will adopt the shape of corresponding equipotential surfaces of the Roche model. It is easy to see that inside the critical Roche lobe these equipotentials quickly become almost spherical;
3. the two previous facts imply that while the peaks of the Hα emission can be affected by asymmetries of the outer part of the disk, the steep wings reflect the motion of the roughly symmetric inner parts of the disk;
4. thanks to high density of the inner parts, the scattering wings of Hα are roughly insensitive to geometry;
5. any asymmetry in the gas distribution of the inner disk is likely to circularize in a few orbital periods due to viscous effects.

Additionally, if the whole disk is elongated and revolving slowly, this global asymmetry is also reflected by the steep wings of the emission. Consequently, the long-term changes of the RVs measured on the Hα emission wings have a lower amplitude (about 10 km s^{-1}) when compared to the pronounced long-term variations observed for the RVs of the H I, He I and Si II absorption cores (about 70 km s^{-1}). Nevertheless, we had to remove the long-term trend from the measured Hα wings RVs before obtaining the clean orbital RV curve.

The time coverage of the available spectra is less uniform than that required for reliable removal of the long-term trend. We attempted to remove the long-term RV variations using the program HEC13 based on a fit via spline functions after Vondrák (1969, 1977)[2]. After a few experiments, as the optimal choice we used the smoothing parameter $\varepsilon = 5 \times 10^{-15}$ through the 5-day

[2] The program HEC13 with simple instructions is freely available at http://astro.troja.mff.cuni.cz/ftp/hec/HEC13

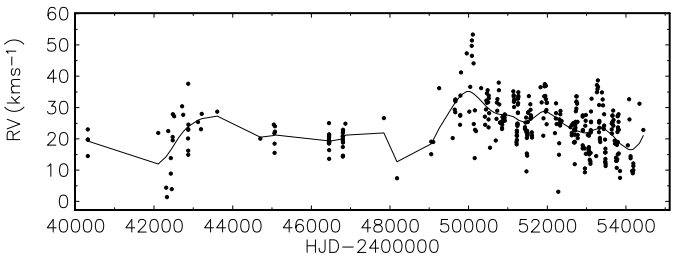

Fig. 5. The time plot of all RVs of the Hα emission wings from photographic and electronic spectra. The solid line shows how the removal of long-term changes was carried out – see the text for details.

moving box-car averaged RV points. The time plot of the Hα emission-wing RVs and the spline fit used are shown in Fig. 5. Note that we defined the spline function using RVs from both the electronic spectra and from digitized Ondřejov photographic spectrograms.

To check how the RVs were prewhitened for the long-term changes, we divided them into subsets spanning not more than some 600 days and derived another RV solution in which different "systemic velocities" were allowed for individual subsets. We omitted a few single RVs which could not be combined into a subset with a sufficient phase coverage. This way, we also allowed for the removal of the long-term RV changes. The resulting RV curve is compared to that based on the residuals from the spline function in Fig. 6 and both trial solutions are compared as solutions 1 and 2 in Table 2. Although the two phase curves in Fig. 6 are not identical, their similarity is obvious and proves the reality of the orbital motion. Moreover, the semiamplitudes of both curves, based on the orbital solutions with the latest publicly available version of the program FOTEL (Hadrava 1990, 2004), are comparable, 6.5 ±0.5 km s^{-1}, and 7.4 ±0.5 km s^{-1}. RVs from the digitized photographic spectra have actually only slightly higher rms errors than those from the electronic ones (5.5 vs. 4.6 km s^{-1}).

As the next step, we re-investigated also all published RVs based on the H I and He I lines. It is a difficult task to use these RVs to improve the value of the orbital period since in the majority of cases these RVs are affected by the contribution of circumstellar shell and its long-term changes. Note also that the RV curve of more accurately measured H I shell lines is distorted, having a sharp maximum and a bump near the RV minimum (see Fig. 7). Those bumps were interpreted by Harmanec (1985) as a influence of a gas stream flowing from the secondary, projected in the certain orbital phases against the primary. In the global oscillation scenario, the disc dynamics is modified when the one-armed spiral pattern forms and important radial components appear (see Okazaki 1997, for instance). It is conceivable that the disturbance pattern in the outer parts of the disc is responsible for the observed distortions of the RV curve and the appearance of the bump. The problem is that in the case of ζ Tau the bump is present also in the periods without long-term variations (see Fig. 3 in Harmanec 1985). Anyhow, it is not quite clear if it is legitimate to compare the RV maxima of such distorted curves with the RV maximum of the sinusoidal RV curve based on the Hα emission wings.

In Table 3 we present three other solutions (denoted 3–5). Solution 3 is based on all H I shell RVs measured on blue photographic spectra and prewhitened for long-term changes with HEC13 ($\varepsilon = 9 \times 10^{-16}$, 5-d normals), solution 4 is based on He I RVs from photographic spectra combined with He I 6678 core

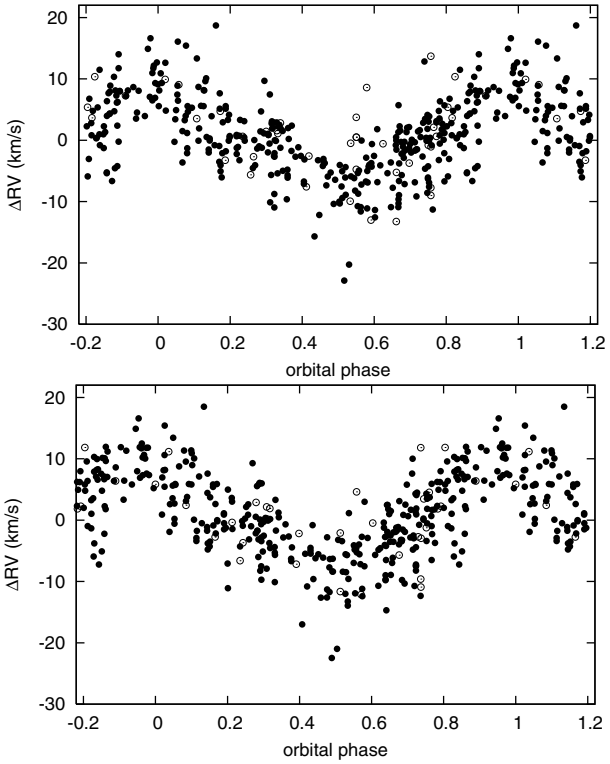

Fig. 6. The orbital RV curve of the Hα emission wings shown for the two different ways of prewhitening for the long-term RV changes. RVs based on the digitized Ondřejov photographic spectrograms are shown by open circles. Note that the systemic velocity was subtracted from the plotted RVs for both phase curves.
Upper panel: Long-term RV variations were removed via spline functions. *Bottom panel*: Long-term variation were removed via orbital solution with FOTEL, in which the data subsets spanning no more than some 600 days were treated as having different systemic velocities.

Table 2. Trial circular-orbit solutions for the RVs measured on the Hα emission wings.

Element	Sol. 1	Sol. 2
P (d)	133.036 ±0.050	132.987 ±0.050
$T_{\text{upper con.}}$	47057.5 ±1.8	47058.8 ±1.8
$T_{\text{RV max.}}$	47024.2 ±1.8	47025.6 ±1.8
K (km s^{-1})	6.53 ±0.47	7.43 ±0.46
rms (km s^{-1})	4.63	4.75
No. of RVs	350	341

In solution 1 long-term variations were removed via spline functions and in solution 2 using different systemic velocities of subsets.

RVs from electronic spectra (prewhitened with $\varepsilon = 1\times10^{-15}$, 5-d normals). Solution 5 is based on a combination of Hα emission-wing RVs (different systemic velocities for less than 600-d long subgroups as in solution 2 were allowed) combined with He I RVs derived via cross-correlation by Jarad (1987).

The results are somewhat confusing and we note that the different solutions for the orbital period in solutions 1–5 are very similar, so the specific choice is not critical for the long-term variations. The interval spanned by the RV observations JD 2415794–JD 2454490, represents 290.95 cycles for the period of 133$^{\text{d}}$.0, and 291.17 cycles for 132$^{\text{d}}$.9. The difference can be caused by the changes in the circumstellar matter. This is illustrated by Fig. 7 where a gradual development of a secondary

Table 3. Trial solutions for the H I shell RVs, He I RVs and a combination of Hα emission-wing RVs with He I RVs measured via cross-correlation in Jarad (1987).

Element	Sol. 3	Sol. 4	Sol. 5
P (d)	132.920	133.000	132.901
	±0.013	±0.034	±0.044
$T_{\text{RV max.}}$	47016.4 ±3.6	47027.2 ±3.5	47027.9 ±1.3
K (km s^{-1})	9.74 ±0.41	7.6 ±1.2	8.29 ±0.61
rms (km s^{-1})	8.09	16.25	4.44
No. of RVs	801	509	178

Solution 3 for the H I shell RVs was formally calculated as an eccentric orbit solution with $e = 0.25$ and $\omega = 305°$, the remaining two solutions are derived for a circular orbit.

RV maximum near the bottom of the RV curve is seen. We therefore conclude that solution 2 of Table 2 represents the best currently available solution and we shall adopt it to define the final binary ephemeris to be used in the rest of this study:

$$T_{\text{RV max.}} = \text{HJD } 2447025.6 + 132^{\text{d}}.987 \times E. \quad (2)$$

Recall that solution 2 is based on the prewhitening based on locally derived shifts of the systemic velocity which is a safer procedure for data with gaps than a somewhat subjective prewhitening via the spline functions. In any case, the difference between the two solutions is not critical for any practical purposes. Comparison of the ephemeris (2) and (1) reveals that the errors of the period and epoch were somewhat underestimated in Harmanec (1984).

Also, we would like to mention that for complex Hα profiles we measured RVs of three distinct absorption cores. We found that all three are involved in the orbital motion and are, therefore, true absorption lines, not "holes" between two neighbouring emission peaks. The middle core (shown in Fig. 7) displays the most distorted RV curve, reminiscent of the one based on the blue H I shell lines but with more noise, perhaps due to blending with telluric lines and poor visibility inside the strong emission.

Adopting tentatively $K = 7$ km s^{-1} and $M_1 = 11\ M_\odot$, we estimated the basic properties of the binary. They are summarized in Table 4 for several plausible values of the orbital inclination.

In spite of various uncertainties in the basic physical properties of the Be primary, it is clear that the secondary is a low-mass object. It could be a hot subdwarf like the secondary of φ Per (Gies et al. 1998). However, in contrast to that binary, we have not detected any sharp emission in the He I 6678 A line which would moving in antiphase to the RV curve of the Be star. Note that according to Hummel & Štefl (2001), such an emission originates in a part of the Be-star disk, facing the hot secondary, which is illuminated by it. Alternatively, the secondary of ζ Tau can also be a normal solar-like main-sequence star. In any case, the direct detection of the secondary will be very difficult.

5.2. Spectrophotometric and photometric orbital phase-locked changes

Contrary to the RV changes, possible orbital phase-locked variations of other observables were not frequently studied in the past. Pavlovski & Božić (1982) reported occasional decreases of brightness in the season 1981/82 which coincided almost exactly with the moment of the expected superior conjunctions based upon the Harmanec (1984) ephemeris as shown by Božić & Pavlovski (1988). Most recently Pollmann & Rivinius (2008)

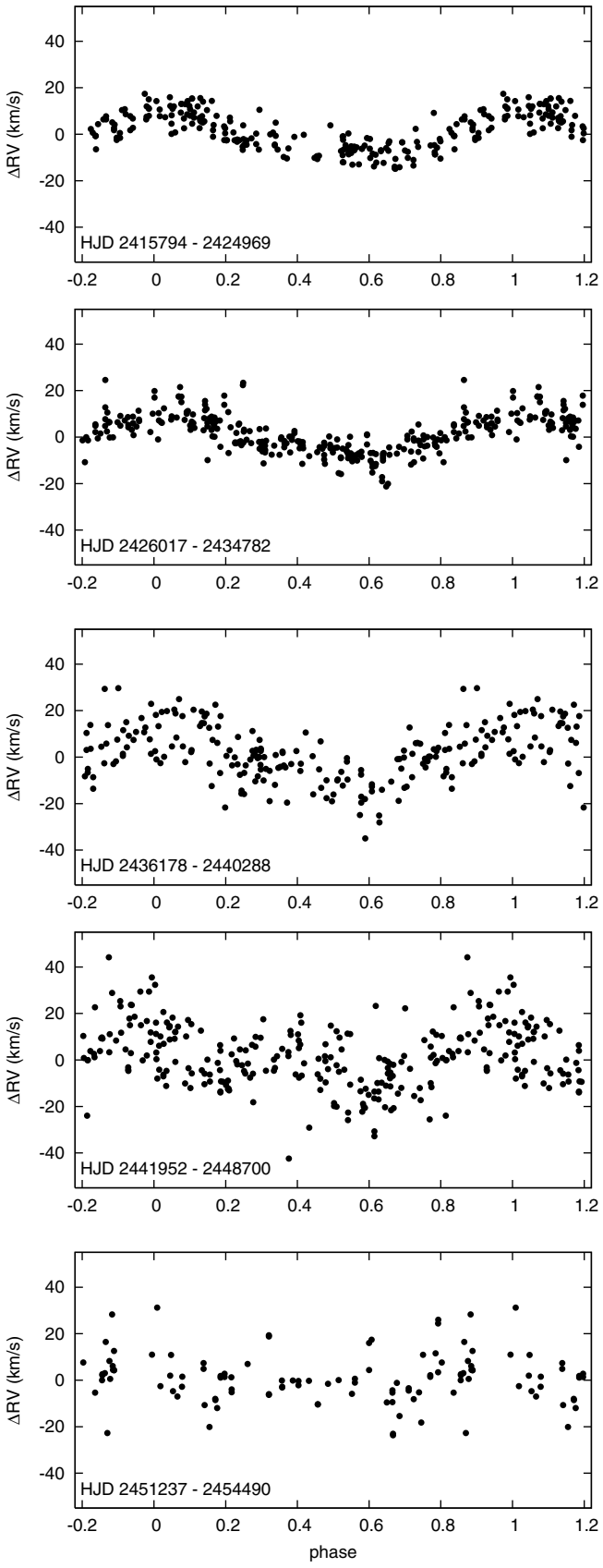

Fig. 7. Phase plot of several subsets of H I shell RVs, prewhitened for the long-term changes, vs. orbital phase. One can see the gradual development of the bump near the minimum RV. In the *bottom panel*, the RVs of the Hα core (*middle* one for the complex profiles) are shown. The ephemeris $T_{\mathrm{RV\,max.}}$ = HJD 2415643.3 + 132$^{\mathrm{d}}$.9735 × E was used.

Table 4. Basic properties of the binary system estimated for K = 7 km s^{-1} and M_1 = 11 $M_\odot$ and for several plausible orbital inclinations.

i (deg.)	M_2/M_1	M_2 ($M_\odot$)	A ($R_\odot$)	R_1^{Roche} ($R_\odot$)	R_2^{Roche} ($R_\odot$)
90	0.079	0.87	250.1	154.4	46.1
80	0.081	0.89	250.2	154.1	46.3
70	0.085	0.93	250.5	153.1	47.1
60	0.092	1.02	251.1	151.5	48.4

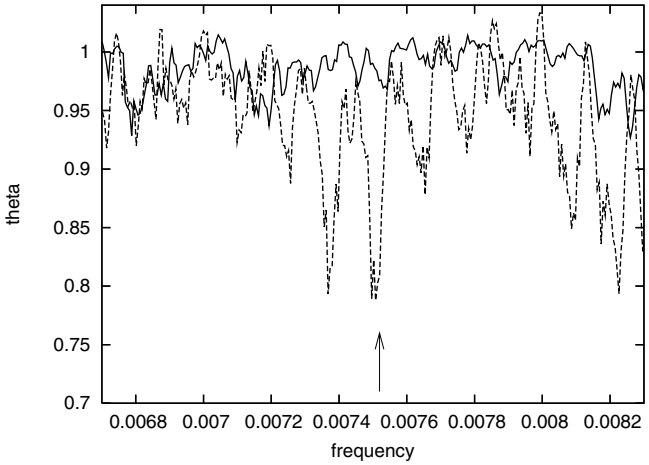

Fig. 8. Stelingwerf's PDM periodogram of the V/R ratio prewhitened for the long-term changes using spline functions. Solid line shows the analysis of simple double-peaked profiles, the dashed line the triple-peaked profiles. The arrow denotes the frequency of the orbital period.

found a 69.3 ± 0.2 d cycle in V/R variations between JD 2452100 and JD 2453500.

To investigate the orbital modulation of emission lines and light variations the Hα EW and V/R, He I 6678 A EW and intensity, V magnitude, $U-B$ and $B-V$ colours were analysed. The long-term variations were removed using HEC13, and a search for periodicity in the range of periods from 10 to 2000 days was performed using PDM (Stellingwerf 1978). The analysis was done for the whole data set, and separately for two subsets resulting from the division of the data near HJD 2449000. With the exception of the V/R ratio, there are no peaks in the periodograms above the noise level at a frequency corresponding to the orbital period. For the V/R ratio, we analysed also the profiles of different complexities separately. It was found that complex profiles show orbital variations while the simple double-peaked profiles show weak or no orbital variation at all. This is illustrated in Fig. 8 where the PDM periodograms of the V/R ratio for double-peaked and more complex Hα profiles are displayed. For simple profiles, the PDM analysis yields a period of 69$^{\mathrm{d}}$.6. The PDM analysis of all profiles (regardless of complexity) observed before JD 2449000 (HJD < 2449000 subset) gives 66$^{\mathrm{d}}$.5, or 133$^{\mathrm{d}}$.0 with a double-wave curve, and the analysis of all profiles obtained after this date (HJD > 2449000 subset) yields 69$^{\mathrm{d}}$.6 or 139$^{\mathrm{d}}$.1 with a double-wave curve. If complicated profiles are excluded those results do not change significantly.

To check the above-mentioned results, we prewhitened alternatively the V magnitude and V/R data for the long-term changes using the program HEC36 which is based on the Hermite polynomial interpolation scheme as provided in the program

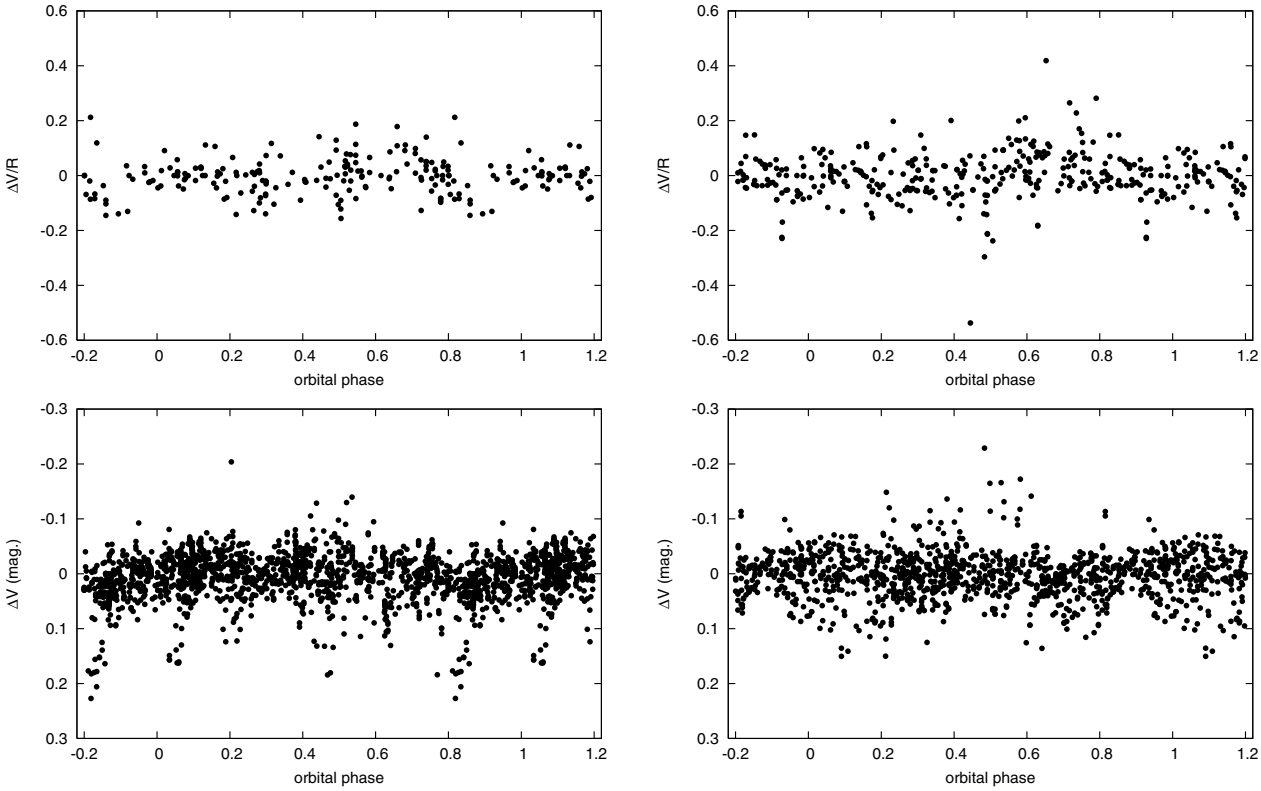

Fig. 9. Phase plots of individual V/R (*upper row*) and V magnitude (*lower row*) observations. Ephemeris from solution 2 are used and long-term changes were removed using Hermite polynomial interpolation scheme. *Left*: HJD < 2449000 subset. *Right*: HJD > 2449000 subset.

INTEP by Hill (1982)[3]. The residuals were then analysed using PERIOD04 (Lenz & Breger 2005). The whole data set as well as HJD < 2449000 and HJD > 2449000 subsets were analysed and simple and complex profiles were treated together. The analysis of the V magnitude data yields several periods in the range 50 to 200 days, while the analysis of V/R data gave similar periods as PDM. Analysis of the complete V/R dataset finds $69\overset{d}{.}2$ as the best period, the HJD > 2449000 subset gives both $69\overset{d}{.}5$, and $66\overset{d}{.}5$ periods, while the analysis of HJD < 2449000 subset does not yield any period in the vicinity of orbital period or in the range 60–70 days.

Orbital phase plots for the V magnitude and V/R ratio, based on individual data points, are shown in Fig. 9. Some orbital modulation of both studied quantities is seen there. To examine the orbital modulation in more detail, the observations were divided into individual observing seasons. For the V/R ratio, only the HJD > 2449000 subset was analysed.

Upon examination of orbital phase plots for individual observing seasons it can be concluded that the orbital light and V/R curves are changing from season to season, both in amplitude and phase. The amplitude of the V/R variation is smaller near the minimum, and larger near the maximum of the long-term RV cycle – see Fig. 10. Due to the relatively small number of measurements during any one season it is difficult to draw conclusions about the changes in phase. The changes in orbital light modulation are more complicated and there is no obvious connection to the long-term cycle. This is a consequence of light decreases that occur at arbitrary orbital phases and of rapid variations of brightness.

[3] The program HEC36 with simple instructions on how to use it is freely available at http://astro.troja.mff.cuni.cz/ftp/hec/HEC36

The period analysis of V/R data revealed the period of 69.6 or a twice longer 139.1-d period exhibiting a double wave phase curve. (We note that Adams (1905) derived a period of 138 days as the best one for the RV variations from the first observed quiet period without long-term changes but the relevance of this coincidence is not clear). Note, however, that the following relation between the orbital and 139.1-d period holds:

$$139.1^{-1} - P(\mathrm{orb})^{-1} = 3019.1^{-1}. \quad (3)$$

Note that the 3019-d "period" is the value comparable to the length of the long-term cyclic change during the last cycles covered by electronic spectra. It is conceivable, then, that the V/R ratio is actually modulated simultaneously by the orbital period and by cyclic long-term changes while the 69/139-d period is an apparent period only, resulting from the beat of the former two.

Another possible explanation of the $69\overset{d}{.}6$ period could be a temporal presence of a blob of material in a Keplerian orbit around the primary, not very far from its Roche lobe. For instance, a blob orbiting around an 11 $M_\odot$ primary with a period of 69.6 days, would be located at an effective distance of 106 $R_\odot$. For the RV semi-amplitude of the primary $K_1 = 7.0$ km s^{-1}, the radius of the Roche lobe around the primary is larger than 150 $R_\odot$ for any orbital inclination between 60° and 90° – see Table 4.

6. Towards physical interpretation of long-term changes

As it was shown in the previous sections, ζ Tau is a very intricate object. In the past, there were several attempts to understand the physical nature of the long-term changes. Struve (1931) suggested that the cyclic long-term RV and V/R variations of some

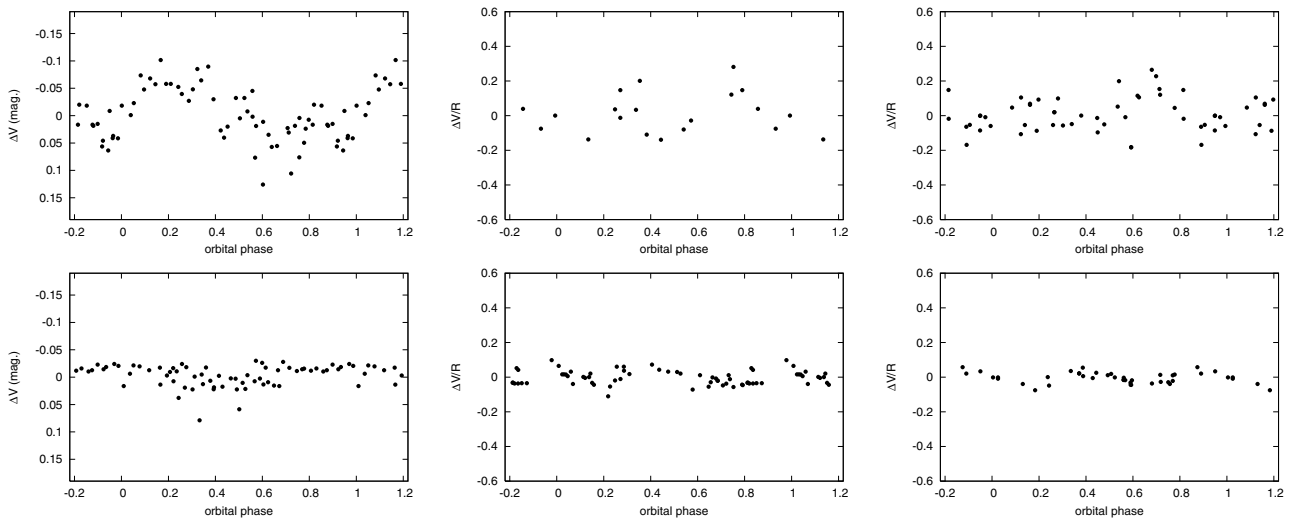

Fig. 10. Orbital phase plots of individual V observations (*left panels*) and the V/R ratio (*central and right panels*) for individual observing seasons. Seasons with larger amplitude of orbital variations (HJD 2450726–2450918, 2451237–2451572 and 2453231–2453482 *from left to right*) are shown in the upper row, and the seasons with smaller amplitude of orbital variations (HJD 2451075–2451278, 2451850–2452002 and 2453611–2453844) are plotted in the lower row.

Be stars could be explained if the circumstellar disk temporarily adopts an elongated (elliptical) shape and slowly revolves around the star. Johnson (1958) was the first who pointed out that such a revolution of an elliptical envelope is a direct analogy to the binary apsidal motion caused by the mass distribution inside the star. He argued that the apsidal period of the elongated envelope $P_{\rm long}$ can be calculated as

$$P_{\rm long} = P\frac{A^2}{R^2}\left(\frac{1}{k\cdot w}\right), \quad (4)$$

where P is the orbital period of the particles in the elliptical envelope, A the mean distance of the disk particles from the centre of the star, R the stellar radius, k the usual constant of internal structure of the star, and w is the ratio of centrifugal to gravitational force. Using values typical for Be stars, he found that formula (4) gives periods of the order of several years as observed. McLaughlin (1961) indeed showed for a simple geometrical model of a thin elliptical envelope that a slow revolution of such a structure leads to parallel RV and V/R variations of emission lines and RV variations of the shell absorption lines, in agreement with available observations. Kříž & Harmanec (1975) pointed out that an elongated envelope could be formed by a short-living inflow of material towards the Be star from its binary companion. They found from particle-trajectory calculations that such an envelope would revolve thanks to the attractive force of the binary component even around a point-like star, i.e., without the effect of the classical apsidal motion. In recent years, the most popular explanation of the long-term spectral changes of Be stars has been that the apparent asymmetry of the disk is a one-armed oscillation pattern as suggested by Kato (1983). The wide acceptance of Kato's model stems from the fact that it was quantitatively developed in a number of studies – for instance by Okazaki (1991), Okazaki (1996), Okazaki (1997), Papaloizou et al. (1992), Papaloizou & Savonije (2006), Fiřt & Harmanec (2006), Ogilvie (2008) and Carciofi et al. (2009) among others. In those studies, two different effects were considered (alternately and together) to maintain the oscillations: (1) the force of the radiative pressure gradient, and (2) the quadrupole term of the gravitational potential that arises from rotational flattening; see Johnson (1958). Ogilvie (2008) used a 3-D modelling of the oscillation and concluded that the 3-D effects are substantial and lead to the observed prograde rotation of the density enhancement (Vakili et al. 1998) even if the radiative force is neglected and the quadrupole mode of the gravitational potential is negligible.

In contrast to the above-mentioned studies which simply postulate the existence of a circumstellar disk around *a single star* and study its perturbations, Kříž & Harmanec (1975) tried the explain the very origin and time evolution of the disk via a model of a discontinuous mass transfer from a secondary star in a binary system. It is true that their model postulated a Roche-lobe filling secondary and no such a large cool secondary was detected – see, e.g., Floquet et al. (1989). However, their idea of putting a blob of material into an orbit around a rapidly rotating B star is more general. First, such inflow of material could occur in the form of a density enhancement in the stellar wind from a very hot O subdwarf secondary (like the secondary of a similar Be system φ Per), or in the form of coronal mass ejections from a solar-like, chromospherically active secondary. Note also that Harmanec et al. (2002a) showed that even if the gas forming the Be envelope is outflowing from the rapidly rotating B star which is a member of a binary without any mass transfer, the outflow will *not occur* from the whole stellar equator but only from the rotational Lagrangian point L_1 facing the secondary. They also demonstrated via 3-D gasdynamical modelling that this can lead to the formation of an envelope around the B star.

Unfortunately, no quantitative modelling as that carried out for one-armed oscillation model has been performed for the alternative idea of Kříž & Harmanec (1975). Since the binary character of ζ Tau is rather firmly established, we consider a quantitative investigation of their scenario to be important and intend to present our first effort along this direction in a follow-up study.

To inspire future observational effort, we emphasize that both alternative models would make definite predictions for polarization changes, and that time variable polarization would need to be analysed in conjunction with the spectral data in order to fully test possible options.

7. Conclusions

Thanks to rich series of new spectroscopic, spectrophotometric, photometric and interferometric observations and to a critical compilation of published observational data it was possible to document the pattern of the variations of ζ Tau on several distinct time scales.

Our principal results are summarized below:

1. During the last 100 years ζ Tau has gone through three active stages with pronounced long-term variations and two quiet stages. We found that the time intervals when pronounced long-term variations occur coincide with the presence of a strong Balmer emission and that they cease with the decrease of its strength. During the intervals of the long-term activity, RV and V/R variations are in phase, while the brightness and the emission strength display more complex behaviour, obviously partly affected also by changes on shorter time scales. The apparent correlation between the brightness and emission strength changes in time.
2. More complicated Hα profiles, with additional blue- and redshifted absorption components (which all share the orbital motion of the Be primary) are always observed on the rising branch of the long-term V/R cycles when the shell lines become weak and the emission becomes consequently stronger.
3. Measuring the RVs on the steep wings of the Hα emission and utilizing different techniques of data prewhitening, we provided a rather firm proof that the Be star ζ Tau is indeed the primary component of a binary system with an essentially circular 133-d orbit and a semiamplitude of 7.4 ± 0.5 km s^{-1}. We derived an improved binary ephemeris.
4. We discovered mild and complicated phase-locked V/R and brightness variations and demonstrated that they change from season to season. The amplitude of the orbital V/R variations was found to attain a maximum and minimum near the maxima and minima of the long-term cycles, respectively.

Acknowledgements. D. Ruždjak acknowledges the possibility to digitize the Ondřejov photographic spectra with the microdensitometer of the Astronomical Institute of the Slovak Academy of Sciences at Stará Lesná, help and hospitality provided by Dr. J. Zverko, V. Kollár, Dr. R. Komžík and Dr. M. Vaňko there. We thank Dr. S. Ilovaisky who provided us with accurate mid-exposure times for the Observatoire de Haute Provence photographic spectra studied by Dr. Hubert-Delplace. She kindly helped us to resolve some larger differences in the dates of her plates and the list provided by Dr. Ilovaisky. We are also obliged to Drs. G. Burki, H. F. Haupt, J. Paparo, J. R. Percy, and A. Schroll, and Messrs. C. Buil, M. Muminović and M. Stupar who provided us with their unpublished individual observations of ζ Tau. We gratefully acknowledge the use of spectrograms of ζ Tau from the public archives of the Elodie spectrograph of the Haute Provence Observatory and C. Buil Castanet Tolosan Observatory. Observations at Ritter Observatory are supported in part by NSF PREST grant AST-0440784. We thank the Ritter observing team, and particularly director Nancy Morrison, for substantial assistance with obtaining these observations. A detailed criticism and a careful review of the previous versions of the manuscript by an anonymous referee helped us to improve the presentation and sharpen the arguments. The research of the Czech authors was supported by the grants 205/03/0788, 205/06/0304, and 205/08/H005 of the Czech Science Foundation and also from the research project AV0Z10030501 of the Academy of Sciences of the Czech Republic, from the research plan J13/98: 113200004 of Ministry of Education, Youth and Sports *Investigation of the Earth and Universe* and later also from the Research Program MSM0021620860 *Physical study of objects and processes in the solar system and in astrophysics* of the Ministry of Education of the Czech Republic. We acknowledge the use of the electronic bibliography maintained by the NASA/ADS system and by the CDS in Strasbourg.

References

Abt, H. A., & Levy, S. G. 1978, ApJS, 36, 241
Adams, W. S. 1905, ApJ, 22, 115
Alvarez, M., & Schuster, W. J. 1981, Rev. Mex. Astron. Astrofis., 6, 6, 163
Andrillat, Y., & Fehrenbach, C. 1982, A&AS, 48, 93
Aydin, C., Hack, M., & Islik, S. 1965, Mem. Soc. Astron. Ital., 36, 331
Ballereau, D., Alvarez, M., Chauville, J., et al. 1987, Rev. Mex. Astron. Astrofis., 15, 29
Ballereau, D., Chauville, J., Hubert, A. M., et al. 1992, IAU Circ., 5539, 1
Banerjee, D. P. K., Rawat, S. D., & Janardhan, P. 2000, A&AS, 147, 229
Bossi, M., & Guerrero, G. 1989, Informational Bulletin on Variable Stars, 3326, 1
Božić, H., & Pavlovski, K. 1988, Hvar Observatory Bulletin, 12, 15
Božić, H., Harmanec, P., Horn, J., et al. 1995, A&A, 304, 235
Carciofi, A. C., Okazaki, A. T., le Bouquin, J., et al. 2009, A&A, 504, 915
Dachs, J., Hummel, W., & Hanuschik, R. W. 1992, A&AS, 95, 437
Delplace, A. M. 1970a, A&A, 7, 68
Delplace, A. M. 1970b, A&A, 7, 459
Fiřt, R., & Harmanec, P. 2006, A&A, 447, 277
Floquet, M., Hubert, A. M., Chauville, J., Chatzichristou, H., & Maillard, J. P. 1989, A&A, 214, 295
Frost, E. B., & Adams, W. S. 1903, ApJ, 17, 150
Galkina, T. S. 1985, Izv. Krymskoj Astrofizicheskoj Observatorii, 72, 72
Gies, D. R., Bagnuolo, Jr., W. G., Ferrara, E. C., et al. 1998, ApJ, 493, 440
Gies, D. R., Bagnuolo, Jr., W. G., Baines, E. K., et al. 2007, ApJ, 654, 527
Gökgöz, A., Hack, M., & Kendir, I. 1962, Mem. Soc. Astron. Ital., 33, 239
Gögköz, A., Hack, M., & Kendir, I. 1963, Mem. Soc. Astron. Ital., 34, 87
Guo, Y. 1994, Informational Bulletin on Variable Stars, 4112, 1
Guo, Y., & Guo, X. 1992, Informational Bulletin on Variable Stars, 3786, 1
Guo, Y., Huang, L., Hao, J., et al. 1995, A&AS, 112, 201
Hadrava, P. 1990, Contributions of the Astronomical Observatory Skalnaté Pleso, 20, 23
Hadrava, P. 2004, Publ. Astron. Inst. Acad. Sci. Czech Rep., 92, 1
Hanuschik, R. W., Kozok, J. R., & Kaiser, D. 1988, A&A, 189, 147
Hanuschik, R. W., Hummel, W., Sutorius, E., Dietle, O., & Thimm, G. 1996, A&AS, 116, 309
Harmanec, P. 1983, Hvar Observatory Bulletin, 7, 55
Harmanec, P. 1984, Bull. astr. Inst. Czechosl., 35, 164
Harmanec, P. 1985, Bull. astr. Inst. Czechosl., 36, 327
Harmanec, P. 1998, A&A, 335, 173
Harmanec, P. 2003, in Publ. Canakkale Onsekiz Mart Univ. 3: New Directions for Close Binary Studies: The Royal Road to the Stars, 221
Harmanec, P., & Božić, H. 2001, A&A, 369, 1140
Harmanec, P., & Horn, J. 1998, J. Astron. Data, 4, 5
Harmanec, P., Horn, J., & Koubský, P. 1982, in Be Stars, ed. M. Jaschek, & H.-G. Groth, IAU Symp., 98, 269
Harmanec, P., Horn, J., & Juza, K. 1994, A&AS, 104, 121
Harmanec, P., Pavlovski, K., Božić, H., et al. 1997, J. Astron. Data, 3, 5
Harmanec, P., Bisikalo, D. V., Boyarchuk, A. A., et al. 2002a, A&A, 396, 937
Harmanec, P., Božić, H., Percy, J. R., et al. 2002b, A&A, 387, 580
Haupt, H. F., & Schroll, A. 1974, A&AS, 15, 311
Herman, R., & Duval, M. 1963, Publications of the Observatoire Haute-Provence, 6, 28
Hill, G. 1982, Publications of the Dominion Astrophysical Observatory Victoria, 16, 67
Horn, J., Kubát, J., Harmanec, P., et al. 1996, A&A, 309, 521
Hubert, A. M., Floquet, M., & Chambon, M. T. 1987, A&A, 186, 213
Hubert-Delplace, A. M., Hubert, H., Chambon, M. T., et al. 1982, in Be Stars, ed. M. Jaschek, & H.-G. Groth, IAU Symp., 98, 125
Hubert-Delplace, A. M., Mon, M., Ungerer, V., et al. 1983, A&A, 121, 174
Hummel, W., & Štefl, S. 2001, A&A, 368, 471
Hynek, J. A., & Struve, O. 1942, ApJ, 96, 425
Jarad, M. M. 1987, Ap&SS, 139, 83
Johnson, H. L., Iriarte, B., Mitchell, R. I., et al. 1966, Communications of the Lunar and Planetary Laboratory, 4, 99
Johnson, H. L., Mitchell, R. I., & Latham, A. S. 1967, Communications of the Lunar and Planetary Laboratory, 6, 85
Johnson, M. 1958, Mem. Soc. Royale Sci. Liège IV. Ser, 20, 219
Juza, K., Harmanec, P., Božić, H., et al. 1994, A&AS, 107, 403
Kato, S. 1983, PASJ, 35, 249
Kaye, A. B., & Gies, D. R. 1997, ApJ, 482, 1028
Köllnig-Schattschneider, E. 1940, Astron. Nachr., 271, 85
Koubský, P., Harmanec, P., Kubát, J., et al. 1997, A&A, 328, 551
Kříž, S., & Harmanec, P. 1975, Bull. astron. Inst. Czechosl., 26, 65
Lenz, P., & Breger, M. 2005, Communications in Asteroseismology, 146, 53
Lockyer, W. J. S. 1936, MNRAS, 96, 230
Losh, H. M. 1932, Publications of Michigan Observatory, 4, 1
McLaughlin, D. B. 1961, JRASC, 55, 73
Mennickent, R. E., Sterken, C., & Vogt, N. 1997, A&A, 326, 1167
Miczaika, G. R. 1953, Zeitschrift fur Astrophysik, 31, 298
Mon, M., Kogure, T., Suzuki, M., et al. 1992, PASJ, 44, 73
Morrison, N. D., Knauth, D. C., Mulliss, C. L., et al. 1997, PASP, 109, 676

Moultaka, J., Ilovaisky, S. A., Prugniel, P., et al. 2004, PASP, 116, 693
Ogilvie, G. I. 2008, ArXiv e-prints, 805
Okazaki, A. T. 1991, PASJ, 43, 75
Okazaki, A. T. 1996, PASJ, 48, 305
Okazaki, A. T. 1997, A&A, 318, 548
Papaloizou, J. C., & Savonije, G. J. 2006, A&A, 456, 1097
Papaloizou, J. C., Savonije, G. J., & Henrichs, H. F. 1992, A&A, 265, L45
Pavlovski, K., & Božić, H. 1982, Hvar Observatory Bulletin, 6, 45
Pavlovski, K., Harmanec, P., Božić, H., et al. 1997, A&AS, 125, 75
Percy, J. R., Ivans, I. I., Fried, R. E., et al. 1994, PASP, 106, 131
Perryman, M. A. C., & ESA 1997, The HIPPARCOS and TYCHO catalogues (The Hipparcos and Tycho catalogues. Astrometric and photometric star catalogues derived from the ESA Hipparcos Space Astrometry Mission, Publisher: Noordwijk, Netherlands: ESA Publications Division, Series: ESA SP Series 1200)
Pollmann, E., & Rivinius, T. 2008, Informational Bulletin on Variable Stars No. 5813, 1
Quirrenbach, A., Buscher, D. F., Mozurkewich, D., Hummel, C. A., & Armstrong, J. T. 1994, A&A, 283, L13
Quirrenbach, A., Bjorkman, K. S., Bjorkman, J. E., et al. 1997, ApJ, 479, 477
Rachkovskaya, T. M., & Nasibova, C. M. 1986, Izv. Krymskoj Astrofizicheskoj Observatorii, 74, 34
Rivinius, T., Štefl, S., & Baade, D. 2006, A&A, 459, 137
Schuster, W. J., & Alvarez, M. 1983, PASP, 95, 35
Schuster, W. J., & Guichard, J. 1984, Rev. Mex. Astron. Astrofis., 9, 141
Shafter, A. W., Szkody, P., & Thorstensen, J. R. 1986, ApJ, 308, 765
Škoda, P. 1996, in Astronomical Data Analysis Software and Systems V, ASP Conf. Ser., 101, 187
Štefl, S., Okazaki, A. T., Rivinius, T., et al. 2007, in Active OB-Stars: Laboratories for Stellare and Circumstellar Physics, ed. A. T. Okazaki, S. P. Owocki, & S. Stefl, ASP Conf. Ser., 361, 274
Štefl, S., Rivinius, T., Carciofi, A. C., et al. 2009, A&A, 504, 929
Stellingwerf, R. F. 1978, ApJ, 224, 953
Slettebak, A., Collins, II, G. W., & Truax, R. 1992, ApJS, 81, 335
Struve, O. 1931, ApJ, 73, 94
Tycner, C., Hajian, A. R., Armstrong, J. T., et al. 2004, AJ, 127, 1194
Underhill, A. B. 1951, Publications of the Dominion Astrophysical Observatory Victoria, 9, 139
Underhill, A. B. 1952, Publications of the Dominion Astrophysical Observatory Victoria, 9, 219
Underhill, A. B. 1953, MNRAS, 113, 477
Underhill, A. B., & van der Wel, T. 1967, in Determination of Radial Velocities and their Applications, ed. A. H. Batten, & J. F. Heard, IAU Symp., 30, 251
Vakili, F., Mourard, D., Stee, P., et al. 1998, A&A, 335, 261
van der Wel, T. 1970, A&A, 4, 341
Vondrák, J. 1969, Bull. astron. Instit. Czechosl., 20, 349
Vondrák, J. 1977, Bull. astron. Instit. Czechosl., 28, 84
Wisniewski, J. P., Kowalski, A. F., Bjorkman, K. S., Bjorkman, J. E., & Carciofi, A. C. 2007, ApJ, 656, L21

Appendix A: Overview of available spectroscopic observations

We secured and reduced 117 electronic spectra of ζ Tau which cover the spectral region containing the Si II 6347 and 6371 A doublet, Hα and He I 6678 A lines. The spectra were obtained at the Ondřejov Observatory and at the Dominion Astrophysical Observatory (DAO hereafter) in the period from 1993 to 2006. Additional 167 Hα echelle CCD spectra were secured at the Ritter Observatory. They have a resolution of 26 000 and the spectrograph is described in Morrison et al. (1997). We also newly reduced a selection of 32 McDonald red CCD spectra, originally used by Kaye & Gies (1997), choosing usually the first and the last spectrogram of each night series. Three spectra of ζ Tau found in the ELODIE archive of the Haute Provence Observatory were also rectified and measured. Moreover, 219 Ondřejov photographic coudé spectra from the years 1967–1992 were digitized with the microdensitometer of the Slovak Academy of Sciences at Stará Lesná. They consist of 36 red spectra, which cover the spectral region containing the Si II 6347 and 6371 A doublet, Hα and He I 6678 A lines and of 183 blue and violet spectra. Additionally, 59 medium-dispersion spectra from Castanet-Tolosan were used for the equivalent-width and line-intensity measurements[4].

The initial reductions of spectra were performed using the IRAF (CCD700, UBC-1, McDonald, and Ritter spectra), MIDAS (Heros spectra) and SPEFO (Reticon and photographic spectra) programs. All subsequent reductions and the RV and spectrophotometric measurements were carried out using the SPEFO reduction program written by the late Dr. J. Horn and recently further developed by Dr. J. Krpata (Horn et al. 1996; Škoda 1996). The only exception is the series of Ritter Hα spectrograms for which NR measured the Hα -emission wing bisector velocities at $\pm$350 km s^{-1} from the line center using the convolution method of Shafter et al. (1986).

A.1. Radial-velocity data files

We carried out a critical compilation of all available RV measurements of H I and He I lines from the literature with the known dates of observations. A large part of these RVs has already been used by Harmanec (1984) but some revision was deemed desirable[5]. These were complemented by additionally published RVs and by our own RV measurements in a large collection of the photographic spectra secured at Ondřejov and in many electronic spectra from the observatories mentioned above. In cases when the original sources give the dates and times of mid-exposures we used the program HEC19 to derive heliocentric Julian dates[6]. The journal of all RVs used in this study is in Table A.1. Julian dates and RVs are tabulated with the accuracy available in the original sources. All Julian dates with 3 or 4 decimal digits are *heliocentric* ones.

A few comments to individual data files follow. The files are identified by the spectrograph Nos. given in Table A.1. Note that we were trying to retain the spectrograph numbers used by Harmanec (1984) but two changes were inevitable as detailed below.

- *Spg. 1* (Adams 1905): The dates of midexposures tabulated in the original paper are given to 1 decimal digit only;
- *Spg. 2* (Losh 1932): The Julian dates tabulated in the original paper are heliocentric ones;
- *Spg. 3&6* (Herman & Duval 1963): Julian dates of all spectra are only given to one decimal place. For the last Perkins Observatory spectrogram it follows from the tabulated date 1957 Dec. 14 that the Julian date is JD 2436187.8, not JD 2436188.8 given in their Table II. We adopted this corrected value but admit that we have no chance to decide whether the date or JD in Table II is in error;
- *Spg. 4 and 8* (Underhill 1952): Harmanec (1984) treated all MtWilson spectrograms as coming from one spectrograph. However, the first five of them are from a prism spectrograph while the remaining ones are from a grating spectrograph. We, therefore, assigned the first 5 spectra as coming another spectrograph, No. 8.
- *Spg. 5* (Underhill 1951): The date of the last few spectrograms Nos. 41717-19, 1951 Jan 29.534, is obviously incorrect: From the comparison with the follow-up study by Underhill (1952) and from the logic we deduce that the correct date should be 1951 Jan 29.234;
- *Spg. 5* (van der Wel 1970): These RV measurements are tabulated in the original paper as mean values from several consecutive spectra for individual Balmer lines. We used the mean RV of H5-H7 and H9-H12 lines, which are available in all spectra. We omitted the RV of H8 line since it seems to be affected by the blending with the He I 3888 line. The tabulated RVs are actually coming from three different grating spectrographs, attached to the 1.83-m a 1.22-m telescopes of the DAO, and to the KPNO 2.1-m reflector. Harmanec (1984) indeed treated them as three different spectrographs Nos. 5, 7, and 8. Considering that in some cases the mean RVs come from both DAO spectrographs, that only a single KPNO RV is tabulated in the original paper, and that all measurements were carried out by the same investigator, we decided treat all these RVs as coming from the 1.83-m DAO spectrograph. The exact dates are only available for three single spectrograms taken on Nov 9, 1964, Dec. 9 a 15, 1964 a (probably) also Jan. 9, 1966. For these spectra, we derived and tabulated HJDs to four decimal digits. All other spectra have only less accurate mean (topocentric) JDs.
- *Spg. 6* (Gögköz et al. 1963): We adopted the H I RVs only for the OHP spectrograms W406 a W567, since RVs from all other OHP spectra were published in more detail by Delplace (1970a). We could not get He I RVs from this study since only their RVs averaged with the RVs of metallic lines are tabulated there.
- *Spg. 6* (Delplace 1970a): We derived the *median* H I RVs for the H9-H18 lines tabulated in the original source. Thanks to Ilovaisky (2006, priv. com.) and Hubert (2008, priv. com.) we were able to derive the accurate HJDs for these spectrograms. This way, we also became aware of a few misprints in Delplace (1970a) paper: Plate W2880 is actually W2879. The date of the plate W3311 is January 3, 1961, not January 13, 1961 as given in the paper. Also the published JD is in error. We therefore also derived the heliocentric corrections of

[4] These spectrograms, obtained and reduced to the form of wavelength calibrated and rectified spectra by their author, a French amateur astronomer C. Buil, are freely available to interested users as ASCII files at `http://www.astrosurf.org/buil/us/becat.htm`

[5] There is one misprint on page 171 of Harmanec (1984): The correct RV at JD ..24563.639 is 34.7 km s^{-1}, not 37.4 km s^{-1} as given there. Moreover, in several cases when more spectra have the same (inaccurate) JD, the H I and He I RVs do not correspond to the same spectrum.

[6] This program which handles data of various forms, together with brief instructions on how to use it, is freely available on the anonymous ftp server at `http://astro.troja.mff.cuni.cz/ftp/hec/HEC19`

Table A.1. Journal of available RV observations of ζ Tau.

Spg. No.	Time interval (HJD−2400000)	No. of H I RVs	No. of He I RVs	Telescope/ Instrument	Source
1	15793.7–16929.6	24	0	Yerkes 1.02-m, Bruce prism spg.	Adams (1905)
2	20408.8–24968.6	160	80	Ann Arbor 0.95-m prism spg.	Losh (1932)
8	26016.7–28450.0	5	1	MtWilson, prism spg.	Underhill (1952)
1	28798.0–30339.8	47	47	Yerkes 1.02-m, Bruce prism spg.	Hynek & Struve (1942)
4	28882.0–34056.7	22	13	MtWilson, grating spg.	Underhill (1952)
5	28962.7–34093.6	63	18	DAO 1.83-m, prism spg.	Underhill (1951, 1952)
3	29893.9–30302.8	52	48	Perkins 1.75-m, grating spg.	Hynek & Struve (1942)
9	33280.4–33772.3	48	44	Heidelberg 0.72-m, prism spg.	Miczaika (1953)
3	33937.7–36188.8	3	0	Perkins 1.75-m, grating spg.	Herman & Duval (1963)
10	36177.5–36598.5	7	0	Merate 1-m, prism spg.	Gökgöz et al. (1962)
6	36918.0	1	0	OHP 1.93-m, grating spg.	Herman & Duval (1963)
6	37205.6–37293.4	2	0	OHP 1.93-m, grating spg.	Gögköz et al. (1963)
6	37209.6–39759.7	112		OHP 1.93-m, grating spg.	Delplace (1970a)
11	37620.5–38421.4	36	0	Merate 1-m, grating spg.	Aydin et al. (1965)
5	38702.0–38744.9	5	0	DAO 1.83&1.22m, grating spg.	van der Wel (1970)
5	39134.6	1	0	KPNO 2.1-m, grating spg.	van der Wel (1970)
7	41952.0–42837.6	23	23	KPNO 1.0-m, grating spg.	Abt & Levy (1978)
12	43867.1–47939.1	44	0	Xing-Long 0.6/0.9-m, grating spg.	Guo et al. (1995)
13	45693.4–46134.4	0	33	StAndrews 0.5-m, grating spg.	Jarad (1987)
14	46451.7–47368.0	6	4	McDonald 2.1-m, CCD grating spg.	Kaye & Gies (1997)
14	46447.6–47159.0	32	32	McDonald 2.1-m, CCD grating spg.	this paper: CCD spectra
15	39852.5–48700.3	147	0	Ondřejov 2.0-m, grating spg.	this paper: blue phg. spectra
16	40316.3–48176.6	38	0	Ondřejov 2.0-m, grating spg.	this paper: red phg. spectra
17	49049.3–51486.6	39	39	Ondřejov 2.0-m, grating spg.	this paper: Reticon spectra
18	51898.4–52727.4	7	7	Ondřejov 2.0-m, grating spg.	this paper: Heros spectra
19	52279.5–54490.4	51	51	Ondřejov 2.0-m, grating spg.	this paper: CCD spectra
20	53077.8–54443.0	20	20	DAO 1.22-m, grating spg.	this paper: CCD spectra
21	49592.7–51572.3	3	3	OHP 1.52-m, Elodie grating spg.	this paper: CCD spectra
22	49779.6–54089.8	167	0	Ritter 1.0-m, echelle spg.	this paper: CCD spectra

RV for both dates and found that it was necessary to increase the published RVs of the plate W3311 for +4.89 km s^{-1}.

- *Spg. 7* (Abt & Levy 1978): These authors tabulated HJDs.
- *Spg. 9* (Miczaika 1953): Julian dates are tabulated to only 1 decimal place but the H I RVs are given to two decimal places.
- *Spg. 10* (Gökgöz et al. 1962): For the spectra from the Merate Observatory, only days of observations are tabulated. Therefore, our deduced Julian dates might be incorrect by one day in some instances.
- *Spg. 11* (Aydin et al. 1965): For these grating spectra, Julian dates of mid-exposures are tabulated to two decimal digits only. We corrected the Julian dates of the spectrograms Nos. 978, 984, 986, 1044, and 1623 for a half-a-day error.
- *Spg. 12* (Guo et al. 1995): Spectrograms with several different dispersions were measured but we take all data as coming from one instrument. The individual RVs have larger-than-usual scatter and we decided to adopt as the most accurate the mean from H4-H6 lines. HJDs are tabulated by the authors.
- *Spg. 13* (Jarad 1987): These He I RVs are derived via cross-correlation and the author tabulates heliocentric MJDs (not HJDs) of mid-exposures.
- *Spg. 14* (Kaye & Gies 1997): These authors studied rapid line-profile variations in a series of McDonald 2.1-m CCD spectrograms and published RVs of the mean Hα, Hβ, He I λ6678, and Fe II λ4924 line profiles from six nights of observing. They found that the superior conjunction predicted by their new RVs occurred $0^{\rm p}.12$ earlier than predicted by ephemeris (1) (Harmanec 1984). When revisiting the data published by Kaye & Gies (1997), we were unable to positively confirm that heliocentric corrections were applied to each of the reduced spectra. We therefore re-reduced the original (raw) spectra to derive new RVs and spectrophotometry values in order to have the most uniform data set possible and to eliminate any chance that the heliocentric correction may be missed in this analysis.

A.2. Spectrophotometric data

Similarly as for RVs, we carried out a critical compilation of all available measurements of the Hα line intensities and equivalent widths (EW) with the known dates of observations. These quantities were also measured on many photographic spectra secured at Ondřejov and electronic spectra from Ondřejov, DAO, OHP, and Castanet-Tolosan observatories. The journal of all spectrophotometric measurements used in this study is in Table A.2.

The individual data files are identified there by letters. All intensities (if not stated otherwise) were measured on published Hα profiles.

Below, we provide a few comments on individual data files:

- *File A* (Underhill 1953): The published profile is a mean profile of three observations and the mean time of observation is given as civil date.
- *File B* (Delplace 1970b): The published profiles are identified by phase of the long-term cycle which is tabulated with EW and plate numbers. The plate numbers 2639 and 3171 given in Table 9 of Delplace (1970b) correspond to the blue (3100–5200 A) plates. Plate denoted 3171 is most probably 3172, while 2639 can be either 2638 or 2659. We have chosen 2659 because for plate 2638 a slightly different phase is given in Table 7 of Delplace (1970b). The accurate times of mid-exposures for the OHP plates were kindly provided by Dr S. Illovaisky.

Table A.2. Journal of available spectrophotometric Hα observations of ζ Tau .

Spg. No.	Time interval (HJD−2400000)	No. of Spectra	Telescope/ Instrument	Source
A	34442.6	1	DAO 1.83-m, prism spg.	Underhill (1953)
B	37367.3–39601.3	10	OHP 1.93-m, grating spg.	Delplace (1970b)
C	38310.5–38422.5	5	Merate 1-m, grating spg.	Aydin et al. (1965)
D	38688.0–38743.9	4	DAO 1.22m, grating spg.	van der Wel (1970)
E	39133.6	1	KPNO 2.1-m, grating spg.	van der Wel (1970)
F	43842.5–47922.5	57	Xing-Long 0.6/0.9-m, grating spg.	Guo et al. (1995)
G	44301.6, 44334.6	2	OHP 1.52-m, grating spg.	Andrillat & Fehrenbach (1982)
H	45200.9–49239.6	8	ESO 1.4-m CAT, grating spg.	Hanuschik et al. (1996)
I	45424.2–45952.6	8	Crimean Observatory 2.6-m	Rachkovskaya & Nasibova (1986)
J	45424.3–45452.2	23	Crimean Observatory 1.22-m, grating spg.	Galkina (1985)
K	45606.0–45620.9	10	SPM 2.1-m, grating spg.	Ballereau et al. (1987)
L	47532.5, 47808.5	2	KPNO coude feed, grating spg.	Slettebak et al. (1992)
M	49316.6, 49642.8	2	GI2T spectrograph	Vakili et al. (1998)
N	49592.7–51572.3	3	OHP 1.93-m, ELODIE	Moultaka et al. (2004)
O	48251.2–49471.0	10	Xing-Long 2.16-m, grating spg.	Guo (1994); Guo et al. (1995)
P	48347.6–52725.3	23	ESO HEROS	Rivinius et al. (2006)
Q	51253.5	1	Mt. Abu IR Obs 1,2-m, grating spg.	Banerjee et al. (2000)
R	51850.5–54174.4	108	0.2-m Schmidt-Cassegrain	Pollmann & Rivinius (2008)
S	53063.5	1	Ritter Observatory 1-m, grating spg.	Wisniewski et al. (2007)
T	40316.3–48176.6	39	Ondřejov 2.0-m, grating spg.	this paper: red phg. spectra
U	46447.6–47159.0	32	McDonald 2.1-m, CCD grating spg.	this paper: CCD spectra
V	49049.3–51486.6	36	Ondřejov 2.0-m, grating spg.	this paper: Reticon spectra
W	51898.4–52727.4	7	Ondřejov 2.0-m, grating spg.	this paper: Heros spectra
X	52204.6–53446.3	59	Castanet-Tolosan 0.212-m and 0.190-m	this paper: Buil CCD spectra
Y	52279.5–54490.4	50	Ondřejov 2.0-m, grating spg.	this paper: CCD700 spectra
Z	53077.8–54443.0	18	DAO 1.22-m, grating spg.	this paper: CCD spectra

- *File C* (Aydin et al. 1965): Julian dates are tabulated to two decimal places (three decimal places in the case of spectrum No. 1898).
- *Files D and E* (van der Wel 1970): For the spectrum taken on Dec. 9, 1964 (Hα profile published by Underhill & van der Wel 1967) we could not decide if it was recorded on 08:27 or 09:40 UT so the mean time was used as the time of observation.
- *File F* (Guo et al. 1995): Only dates of observations are tabulated together with the Hα emission-peak intensities and EW. The exception are 6 spectra obtained in Dec. 1983 for which accurate times of observations are published together with the Hα profiles. Guo et al. (1995) calculated the V/R ratio as $(I_V - 1)/(I_R - 1)$, so their values are not used and the V/R ratio was calculated from the given peak intensities.
- *File G* (Andrillat & Fehrenbach 1982): Four values of the Hα EW and V/R are given. However, Andrillat & Fehrenbach (1982) measured intensities of the emission from the underlying photospheric line. Consequently, their V/R ratio is not comparable to the values used in this study. Times of observations are given as civil dates.
- *File H* (Hanuschik et al. 1996): Julian dates to one decimal place are given by Hanuschik et al. (1988) for five spectra obtained in 1982. Dachs et al. (1992) tabulated the Julian date to three decimal places together with the Hα intensities and EW for a spectrum obtained in 1987. The times of observations for the remaining two spectra are given as civil dates.
- *File I* (Rachkovskaya & Nasibova 1986): Julian dates to three decimal places are tabulated together with the EW and the V/R ratio.
- *File J* (Galkina 1985): Julian dates to three decimal places are tabulated together with the Hα emission-peak intensities, EW and the V/R ratio.
- *File K* (Ballereau et al. 1987): Julian dates to three decimal places are tabulated together with the Hα intensities, EW and the V/R ratio.
- *File L* (Slettebak et al. 1992): The intensities, EW and V/R ratios are tabulated. The times of observations are given as civil dates.
- *File M* (Vakili et al. 1998): Accurate times of observations are tabulated as well as the V/R ratio. Vakili et al. (1998) measured the intensities from the continuum, so their V/R values are not used, and the intensities were measured on the published profiles.
- *File N* (Moultaka et al. 2004): FITS files were downloaded from the ELODIE archive and measured by us.
- *File O* (Guo 1994; Guo et al. 1995): Guo (1994) tabulated the Hα intensities and EW. The times of observations are given as civil dates to three decimal places.
- *File P* (Rivinius et al. 2006): The intensities of the Hα emission peaks and the V/R ratio are tabulated together with HJDs.
- *File Q* (Banerjee et al. 2000): The time of observation is given as civil date.
- *File R* (Pollmann & Rivinius 2008): The Hα profiles are tabulated as intensity versus wavelength. The wavelength range for the time interval JD 2451850.5–2452737.3 is 6545.0–6577.9 A while for JD 2452883.6–2454174.4, the range is 6545.2–6579.8 A. The EWs measured in the Hα profiles from the first time interval are systematically smaller by several A than the ones obtained from the high-resolution spectra secured in about the same time. Consequently, these Pollman's EWs are not used here. The Julian dates are given to one decimal place.
- *File S* (Wisniewski et al. 2007): The time of observation is given as civil date.

Table B.1. Journal of available photometry of ζ Tau with known times of observations.

Station	Time interval (HJD−2400000)	No. of obs.	Passbands	HD of comparison / check star	Source
–	29296.5–29302.4	6	465& 418 nm	36819	Köllnig-Schattschneider (1940)
23	38306.0–38427.8	3	*UBV*	all-sky	Johnson et al. (1966)
95	39061.9–39440.9	2	*UBV*	all-sky	Johnson et al. (1967)
26	39927.4–40286.4	3	*BV*	36589	Haupt & Schroll (1974) and priv.com. to PH
37	41323.6–42735.8	3	*UBV*	all-sky	Burki (1980, priv.com. to PH)
01	43135.4–51513.6	728	*UBV*	36589/37711	Pavlovski et al. (1997) & this paper
30	44656.8–44659.7	3	m_{58}	all-sky	Schuster & Guichard (1984)
04	45646.6–46007.7	11	*UBV*	36589	this paper
20	45715.7–45719.7	5	*UBV*	37711/36589	Percy (1986, priv.com. to HB)
20	46002.8–46010.0	13	*UBV*	37711/36819	Percy (1986, priv.com. to HB)
08	46056.0–48974.2	23	*UBV*	36589	Guo et al. (1995)
49	46496.7–46543.6	23	*UBV*	37711/36819	this paper
15	46820.8–51645.6	1421	*UBV*	36589/37711	this paper
09	47940.4–47941.4	5	*UBV*	36589/37711	Muminović & Stupar (1990, priv.com.)
61	47962.3–49039.8	46	*V*	all-sky	Perryman & ESA (1997)
73	48533.6–48537.7	19	*UBV*	37711/36819	Percy et al. (1994), Paparo (2008, priv.com.)
01	51943.4–54131.4	157	*UBV*	36589/42690	this paper

Individual observing stations are distinguished by running numbers they have in the Prague/Zagreb photometric archives – see column *"Station"*: 01... Hvar 0.65-m reflector, EMI6256 tube; 04... Ondřejov 0.65-m reflector, EMI6256 tube; 08... Xing-Long, China, 0.60-m reflector, EMI 6256B; 09... Sarajevo Čolina Kapa 0.30-m reflector, 1P21 tube; 15... Phoenix-10 APT, SSP-3 photometer, Fairborn; 20... University of Toronto 0.40-m reflector, Optec SSP-3 photometer; 23... Catalina, original *UBV* observations; 26... Haute Provence Observatory 0.60-m reflector, Lallemande tube; 30... San Pedro Mártir 0.84-m & 1.5-m reflector, 6C red filters; 37... Jungfraujoch, Geneva 7-C system observations transformed to *UBV*; 49... Limber Observatory; 61... Hipparcos all-sky H_p photometry transformed to Johnson *V* 73... Piszkéstetö 0.50-m Cassegrain reflector, EMI 9502S tube; 95... Tucson Lunar Planetary Laboratory 0.53-m reflector, 8*C* filters transformed by us to *UBV*.

Table B.2. Accurate Hvar *all-sky* mean *UBV* values for all comparison stars used. These were added to the magnitude differences var.−comp. and check−comp. for data from all stations. For comparison, also the *UBV* magnitudes of 126 Tau from *UBV* all-sky photometry by Johnson et al. (1966) and from 8C all-sky photometry by Johnson et al. (1967) transformed to *UBV* by us.

Station	Star	HD	No. of obs.	*V* (mag.)	*B* (mag.)	*U* (mag.)	$(B-V)$ (mag.)	$(U-B)$ (mag.)
01	HR 1860	36589	741	6.211 ±0.010	6.180 ±0.011	5.788 ±0.013	–0.031	–0.392
01	126 Tau	37711	635	4.853 ±0.011	4.728 ±0.012	4.086 ±0.014	–0.125	–0.642
01	121 Tau	36819	149	5.385 ±0.013	5.305 ±0.013	4.677 ±0.016	–0.080	–0.628
23	126 Tau	37711	3	4.862 ±0.028	4.743 ±0.033	4.108 ±0.045	–0.119	–0.635
30	126 Tau	37711	2	4.857 ±0.003	4.716 ±0.004	4.052 ±0.006	–0.141	–0.664

Appendix B: Photometry

Photoelectric observations used in this study consist of numerous *UBV*, *BV* and *V* photometric measurements (or measurements in other photometric systems which we were able to transform to the Johnson *UBV* system) from 14 different observatories. We used only those published data for which accurate dates of observations are known. The observations span an interval 1961–2007 and consist of both, already published observations and new data obtained by us. Basic information is provided in Table B.1. As seen there, most of the available data sets were secured differentially, relative to either HR 1860 = HD 36819 or 126 Tau = HD 37711 and there are also three data sets based on all-sky photometry.

Special effort was made to derive improved *all-sky* values for all comparison stars used, employing carefully standardized *UBV* observations secured at Hvar over several decades of systematic observations. The new values are collected in Table B.2, together with the number of all-sky observations and the rms errors. They were added to the respective magnitude differences to obtain directly comparable standard *UBV* magnitudes for all stations. We did our best to reduce all the data to the standard Johnson *UBV* system. How well this was possible is explained in the detailed comments on individual data sets below where we provide also other useful pieces of information. It can also be judged by inspecting Table B.3 where we provide the mean *UBV* magnitudes of the check stars observed at individual stations derived relatively to the Hvar all-sky values for HR 1860 or 126 Tau.

Hvar, Ondřejov, Limber, Sarajevo and Xing-Long observations were secured during an international campaign on photometry of Be stars (Harmanec et al. 1982). Those observations were reduced to the standard *UBV* system using the HEC22 computer code (Harmanec & Horn 1998).

– *Observations by Köllnig-Schattschneider (1940):* These 1940 Heidelberg photoelectric observations were obtained with a potassium diode. Several other known variables and binaries were also observed. From a comparison of phase curves for some binaries observed by Köllnig-Schattschneider (1940) with more recent observations we had concluded that the accuracy of these early observations is too low to be valuable in the study of the relatively mild light changes of ζ Tau. Thus, we gave up on

Table B.3. Mean *UBV* values for the check stars used at individual observing stations derived differentially relative to their respective comparison stars (cf. Table B.1). They illustrate how closely the data could be transformed to a comparable standard system.

Station	Star	HD	No. of obs.	V (mag.)	B (mag.)	U (mag.)	$(B-V)$ (mag.)	$(U-B)$ (mag.)
01	126 Tau	37711	971	4.852 ±0.011	4.727 ±0.010	4.085 ±0.013	–0.126	–0.642
04			10	4.852 ±0.019	4.735 ±0.018	4.094 ±0.013	–0.117	–0.641
09			6	4.855 ±0.025	4.735 ±0.026	4.065 ±0.048	–0.120	–0.671
15			1283	4.854 ±0.015	4.722 ±0.013	4.094 ±0.016	–0.132	–0.627
49			23	4.862 ±0.012	4.736 ±0.013	4.130 ±0.013	–0.125	–0.606
01	121 Tau	36819	248	5.382 ±0.013	5.303 ±0.012	4.676 ±0.015	–0.079	–0.627
04			4	5.380 ±0.012	5.311 ±0.016	4.677 ±0.009	–0.069	-0.634
20			12	5.388 ±0.004	5.303 ±0.004	4.688 ±0.008	–0.085	–0.614
73			17	5.379 ±0.010	5.301 ±0.017	4.676 ±0.029	–0.078	–0.625
20	HR 1860	36589	4	6.210 ±0.009	6.174 ±0.009	5.759 ±0.016	–0.036	–0.415

the attempts to transform these observations to the B and V magnitudes and have not used them.

– *Station 01 – Hvar:* These observations were reduced to the standard UBV system via non-linear transformation formulæ using the HEC22 reduction program – see Harmanec et al. (1994) and Harmanec & Horn (1998). The first part of them was secured in the course of the international campaign on photometry of Be stars (Harmanec et al. 1982) and has already been analyzed by Pavlovski et al. (1997), Pavlovski & Božić (1982) and by Božić & Pavlovski (1988) and published in detail by Harmanec et al. (1997). The 1999–2007 observations are published and analyzed for the first time here. Observations since 2000 were reduced with a more sophisticated HEC22 rel.16 program which can also model time variation of linear extinction coefficients in the course of observing nights.
– *Station 04 – Ondřejov:* These *UBV* observations were secured by several Ondřejov astronomers and reduced to the standard *UBV* magnitudes with the HEC22 program.
– *Station 08 – Xing-Long:* These *UBV*observations were also secured as part of the international campaign on photometry of Be stars. They represent normal points of several individual observations for each night. They were reduced and transformed to the standard *UBV* system by Guo et al. (1995) using the HEC22 program.
– *Station 09 – Sarajevo:* These *UBV* observations were obtained at the Čolina Kapa mountain station by Messrs. M. Muminović and M. Stupar and provided as a part of the international campaign. We reduced these data the to standard *UBV* system using the HEC22 rel.16 program and non-linear seasonal transformation formulæ.
– *Station 15 – Fairborn:* These *UBV* observations were secured at the request of D. McDavid with the 0.25-m Automatic Photometric Telescope (APT). They were reduced via linear transformation formulæ into the standard *UBV* system by the APT service, a non-profit service directed by Professor Michael Seeds.
– *Station 20 – Toronto:* This limited set of *UBV* observations comes from the photometric archive of Dr. J.R. Percy. They were reduced to the *UBV* system via linear transformation formulæ by their author. The observations were obtained in support of the international program but never published.
– *Station 23 – Catalina:* These original UBV all-sky observations were published with dates of observations by Johnson et al. (1966). We converted their tabulated JDs into HJDs.
– *Station 26 – Haute Provence:* A mean value of three 1968-1969 observations was published by Haupt & Schroll (1974) and the individual B and V magnitude differences were communicated privately to P. Harmanec. The times of observations are known with an accuracy of ±0.1 d. The observations were reduced to the *UBV* system by their authors and we only added the Hvar mean all-sky values to their magnitude differences.
– *Station 30 – San Pedro Mártir:* These all-sky observations were secured with the 6 red filters by Schuster & Guichard (1984). We cannot transform these observations to the standard *UBV* system and we only used the m_{58} magnitude (which is reasonably close to Johnson V) to monitor the long-term changes.
– *Station 37 – Jungfrauhof:* These all-sky 7-C observations were secured in the Geneva photometric system and kindly put at our disposal by Dr. G. Burki (priv. com. to PH). We transformed them into *UBV* magnitudes using the transformation formulæ derived by Harmanec & Božić (2001).
– *Station 49 – Limber Observatory:* These observations were secured and reduced by David McDavid at his private observatory as a part of the international campaign on photometry of Be stars relative to 126 Tau. We only added the standard Hvar *UBV* all-sky values of 126 Tau of Table B.2 to the magnitude differences derived by DMD.
– *Station 61 – Hipparcos:* These observations were reduced to the standard V and B magnitudes via the transformation formulæ derived by Harmanec (1998). Since the star underwent long-term colour variations over the period 1989–93, covered by Hipparcos observations – as illustrated by Fig. B.1 – we proceeded in the following way: We first derived suitably chosen normal points of observational data secured shortly before, during and shortly after the Hipparcos observations at several stations. It turned out that the $B-V$ changes were best described by 100-d normals while the more pronounced $U-B$ variations were characterized by 15-d normals. Then we derived smooth lines passing through the normal points with the help of a non-linear interpolation based on Hermite polynomials using program INTEP by Hill (1982). With them, we derived the appropriate values of $B-V$ and $U-B$ for the times of individual H_p observations and these values were used to transform individual Hipparcos observations to Johnson V after Harmanec (1998). The resulting V magnitudes are compared with the true V observations from other stations in Fig. B.2. A very satisfactory agreement is seen there. Note also that Figs. B.1 and B.2 illustrate the level

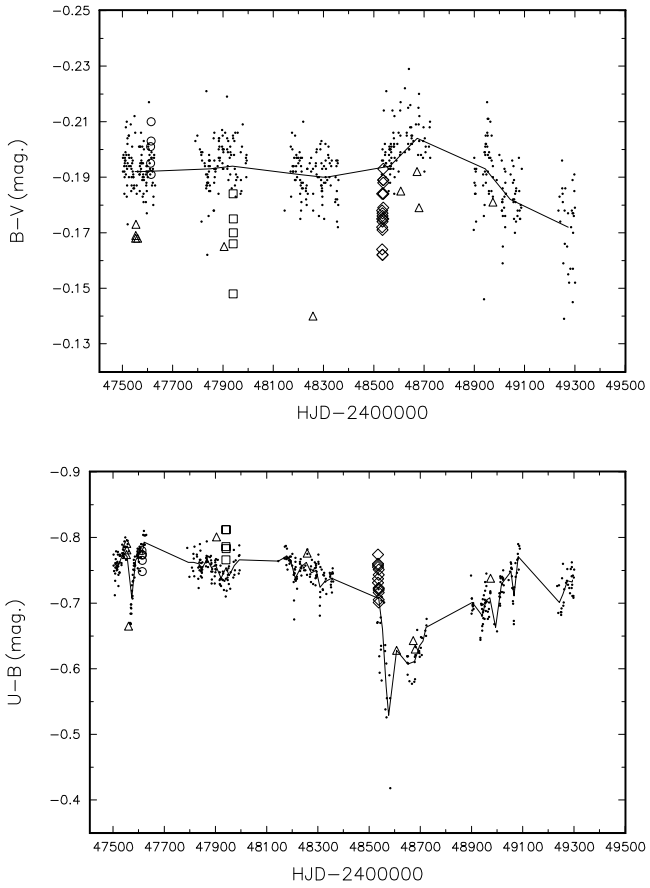

Fig. B.1. Time plots of $B-V$ and $U-B$ indices of ζ Tau based on various observations secured over the time interval covered by the Hipparcos H_p observations and shortly before and after it. Following notation is used to distinguish data from various stations identified in Table B.1: 01... empty circles, 08... empty triangles up, 09... empty squares, 15... small black dots, 73... empty diamonds. The solid lines are connecting the normals points over 100 d in $B-V$ and over 15 d in $U-B$ – see the text for details.

of (dis)agreement of magnitudes and indices from individual observing stations.

– *Station 73 – Piskéstetö:* These *UBV* observations, used in the paper by Percy et al. (1994), were obtained by Dr. M. Paparo and kindly put at our disposal for analyses in the form of magnitude differences ζ Tau – 126 Tau and 121 Tau – 126 Tau, transformed to the standard *UBV* system and corrected for differential extinction. These observations will be later published by their author and are not, therefore, included in Table 4. Regrettably, the other set of photometry used by Percy et al. (1994), obtained at Braeside Observatory, is not available.

– *Station 95 – Tucson:* These 8C all-sky observations were obtained and published by Johnson et al. (1967) and we transformed them to the *UBV* magnitudes using the transformation formulæ derived by Harmanec & Božić (2001).

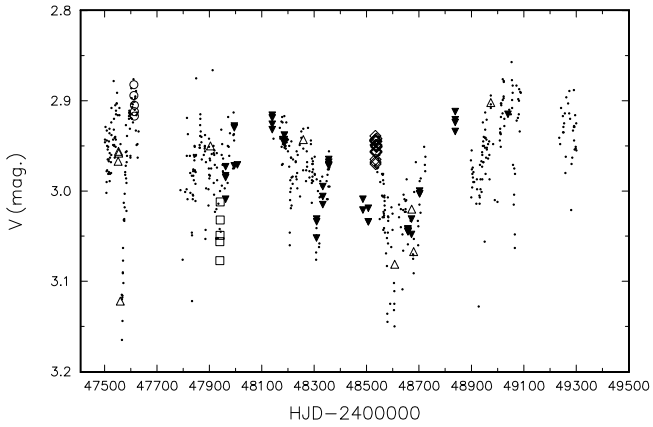

Fig. B.2. Time plots of V photometry of ζ Tau based on various observations secured over the time interval covered by the Hipparcos H_p observations and shortly before and after it. Following notation is used to distinguish data from various stations identified in Table B.1: 01... empty circles, 08... empty triangles up, 09... empty squares, 15... small black dots, 73... empty diamonds. The solid lines are connecting the normals points over 100 d in $B-V$ and over 15 d in $U-B$. Hipparcos H_p magnitudes transformed to Johnson V are shown by black triangles down. See the text for the details.